

**DEVELOPMENT AND CHARACTERIZATION OF VIRAL
VECTORS FOR STRESS-DEPENDENT TRANSGENE EXPRESSION
IN NEURONS**

A Dissertation
Presented to
The Academic Faculty

by

Angel J. Santiago-Lopez

In Partial Fulfillment
of the Requirements for the Degree
Doctor of Philosophy in BioEngineering

Georgia Institute of Technology
May 2021

COPYRIGHT © 2021 BY ANGEL J. SANTIAGO-LOPEZ

**DEVELOPMENT AND CHARACTERIZATION OF VIRAL
VECTORS FOR STRESS-DEPENDENT TRANSGENE EXPRESSION
IN NEURONS**

Approved by:

Dr. Robert Gross, Advisor
Department of Biomedical Engineering
Georgia Institute of Technology

Dr. Michelle LaPlaca
Department of Biomedical Engineering
Georgia Institute of Technology

Dr. Jae-Kyung (Jamise) Lee
Department of Physiology and
Pharmacology
University of Georgia

Dr. Ravi Kane
School of Chemical and Biomolecular
Engineering
Georgia Institute of Technology

Dr. Mark Prausnitz
School of Chemical and Biomolecular
Engineering
Georgia Institute of Technology

Date Approved: December 11th, 2020

To my parents, Juan Santiago Gómez and Maritza López Rivera

ACKNOWLEDGEMENTS

Thanks to my advisor Dr. Robert Gross for giving me the opportunity to finish my degree in his group and for the guidance, motivation, and perspective on how to navigate research problems. I am thankful for the freedom to pursue new research projects and gain experience in grantsmanship as a graduate student.

I am thankful for the mentorship and support of Dr. Claire-Anne Gutekunst — from jumping over walls (literally) to find reagents for my experiments to advocating for me when the institutions couldn't decide how to pay for my stipend. This work would not have been possible without her support. Thank you.

Thanks to my thesis committee members — Dr. Michelle LaPlaca, Dr. Jamise Lee, Dr. Ravi Kane, and Dr. Mark Prausnitz for their feedback and insights into this project as well as for their support in fellowship applications and other aspects of my PhD program. I would also like to express my most sincere appreciation to Dr. Andrés García and Laura Paige for helping me navigate the many “struggles” as a BioE PhD student.

My work in the Gross Lab wouldn't have been possible without the help of Dr. Ken Berglund. Ken's resourcefulness was instrumental for my progress in this project and the many offshoots. I would also like to express my gratitude to members of the Gross Lab and the Department of Neurosurgery at Emory, particularly those who helped me get started in the lab: Alejandra Fernandez, Sang-Eon Park, Matt Stern, Mark Connolly, Thomas Shiu, and Kaavya Mandi.

I had the privilege of working with many students throughout my PhD. Each of you taught me how to become a better leader, communicator, teacher, and mentor. In particular, I want to give special thanks to Alex Nazzari for catalyzing the early stages of this project.

I am grateful for the support and sponsorship from my undergraduate research mentors and advisors: Dr. Enrique Meléndez, Dr. José Vera, Dr. Andrew Lyon, Dr. Sid Jhunjhunwala, and Dr. Robert Langer. To all, thanks for opening the doors so that I could pursue a career in science.

I want to acknowledge the support from my professional network and career mentors: Dr. Alejandro Toro (SMDP-Biotech), Dr. Giovanna Guerrero-Medina and Dr. Mónica Feliú-Mojer (Yale Ciencia Academy), and Dr. Corey Harwell (Neuroscience Scholars Program).

Finally, I want to thank those in my inner circle — the ones who fuel my drive. To my parents, Maritza López Rivera and Juan Santiago Gómez, for their total commitment to my education and well-being. To my significant other, Mónica Pérez-Cuevas, for her unconditional support as a friend, writing partner, study partner, and life coach. To my close friends, Adrian Ildefonso, Yoshitaka Sei, Song Ih Ahn, Legna Figueroa-Cosme, and Ricardo Cruz-Acuña, for their support and the countless coffee breaks, Cuban cocktails, and Korean barbecue. Thanks.

This work was supported by NSF Graduate Research Fellowship, the Georgia Tech Presidential Fellowship, the NIH-NINDS T32 Predoctoral Fellowship in Neurology, the Emory URC, and the NIH-NINDS R21-NS112740-01.

TABLE OF CONTENTS

ACKNOWLEDGEMENTS	iv
LIST OF TABLES	viii
LIST OF FIGURES	ix
LIST OF SYMBOLS AND ABBREVIATIONS	xiv
SUMMARY	xvi
CHAPTER 1. Introduction	1
1.1 Motivation	1
1.2 Dissertation structure	3
CHAPTER 2. Background	4
2.1 Cellular Responses to Proteostasis Dysfunction	4
2.1.1 Introduction to the Unfolded Protein Response	4
2.2 The PERK Arm of the Unfolded Protein Response	7
2.2.1 Physiological Implications of PERK/ATF4 Signaling	7
2.2.2 Effector response by ATF4	9
2.2.3 Relevance of PERK/ATF4 Signaling in Neurodegeneration	11
2.3 Experimental Modulation of PERK/ATF4 Signaling	14
2.3.1 Pharmacological modulation	14
2.3.2 Genetic modulation	17
2.4 Experimental Detection of PERK/ATF4 Signaling	18
2.4.1 Conventional molecular biology techniques	18
2.4.2 Fluorescent and luminescent reporters	18
2.4.3 Transgenic mouse reporter lines	20
CHAPTER 3. Development and Characterization of Stress-Dependent Expression Vectors in Neurons	23
3.1 Introduction	23
3.2 Methods	24
3.3 Results	28
3.3.1 AAVs with ATF4-based translational control allow for stress-dependent transgene expression in neurons	29
3.3.2 Kinetic monitoring of ER stress in neurons	33
CHAPTER 4. Kinetic Monitoring of Neuronal Stress in Models of Proteostasis Impairment	37
4.1 Introduction	37
4.2 Methods	40
4.3 Results	44
4.3.1 Neuronal stress response to proteasome inactivation	44
4.3.2 Neuronal stress response to phosphatase inhibition	47

4.3.3	Mutant α -synuclein overexpression elicits a neuronal stress response	49
4.3.4	Mutant α -synuclein influences the neuronal response to ER stress	50
CHAPTER 5. Efficacy Assessment of Stress-dependent MANF Expression		55
5.1	Introduction	55
5.2	Methods	56
5.3	Results	59
5.3.1	Characterization of ATF4-MANF constructs	59
5.3.2	MANF cytoprotection in an in vitro model of cellular stress	60
CHAPTER 6. Discussion and Recommendations for Future Work		62
6.1.1	Insights into neuronal proteostasis	62
6.1.2	Insights into the influence of α -synuclein on ER stress	64
6.1.3	Opportunities for added functionality as a reporter construct	66
6.1.4	Opportunities for use as a stress-responsive gene therapy	67
6.1.5	Opportunities for a cell non-autonomous therapeutic approach	68
Conclusions		70
APPENDIX A. Method Summary for Neurite Analysis Using CellProfiler		71
APPENDIX B. PhD Work Summary (2014-2020)		72
REFERENCES		73

LIST OF TABLES

Table 1	Pharmacological modulators of the UPR in mammalian cells	17
Table 2	ATF4-based expression vectors	26
Table 3	Literature review summarizing the neuroprotective efficacy of MANF	56

LIST OF FIGURES

- Figure 1 The unfolded protein response (UPR) is controlled by three transmembrane sensors in the ER. Activation of the ATF6 arm leads to the nuclear translocation of cleaved ATF6. Similarly, activation of PERK leads to a global halt in protein translation except for a select number of mRNAs such as *ATF4*. IRE1 arm exerts corrective functions via splicing of *XBPI* mRNA. Collectively, activation of the UPR leads to an overall increase in the cellular capacity to manage proteostasis. Created with BioRender. 6
- Figure 2 Intracellular sensors located at the ER membrane detect misfolded proteins and elicit a cellular response. The dissociation of BiP following the interaction with misfolded proteins leads to the dimerization of PERK (protein kinase R (PKR)-like endoplasmic reticulum kinase) and its activation by autophosphorylation. PERK subsequently activates eIF2 α , driving an imbalance in the translational machinery that leads to the selective translation of ATF4. Created by Angel Santiago-Lopez with BioRender. 8
- Figure 3 Human *ATF4* initial coding segment sequence including upstream open reading frames (uORFs) for stress-responsive translational control. Ribosome scanning downstream of uORF2 leads to the translation of ATF4 given the overlap between ATF4 main open reading frame and uORF3 9
- Figure 4 Downstream effects of ATF4 induction following activation of the unfolded protein response. Transcriptional programs led by ATF3, CHOP, and ATF5 control cellular fate decisions such as death or survival. Indirect effects of ATF4 activity influence proteostasis functions such as protein degradation (autophagy) and protein synthesis rates. Adapted from ⁴⁵ 10
- Figure 5 Immunohistochemical examination of markers for the PERK/ATF4 arm of the unfolded protein response (active PERK and eIF2 α) in tissue from patients with confirmed clinical Parkinson's Disease. Adapted from ⁴⁶ 12
- Figure 6 Tunicamycin (TM) structure. TM inhibits protein N-glycosylation in cells leading to accumulation of unfolded proteins in the ER and induction of the unfolded protein response. From Charlesy, Public Domain 15

Figure 7	Thapsigargin (TG) structure. TG inhibits the SERCA pump creating a calcium imbalance which induces the unfolded protein response. From Charlesy, Public Domain	16
Figure 8	Cellular reporters of UPR activation via IRE1 or PERK signaling. (A) Selective XBP1 splicing upon UPR activation via IRE1 leads to a fluorescent readout. (B) Selective translation of ATF4 following the phosphorylation of eIF2 α by PERK generates a PERK-based fluorescent readout. Adapted from ⁸⁴	19
Figure 9	Application of an IRE1 reporter transgenic model to monitor UPR activation at different stages of development. Adapted from ⁸⁶	21
Figure 10	Application of a PERK/ATF4 reporter transgenic model to monitor UPR activation in a pharmacological model of liver fibrosis. Adapted from ⁸⁷	22
Figure 11	Summary of major steps in primary neuronal cultures. Dissected tissue is subjected to enzymatic digestion followed by mechanical dissociation. Cell suspension is cleared by cell straining and media exchange. Created by Angel Santiago-Lopez with BioRender.	25
Figure 12	Process summary for the production of viral vectors. Expansion of the host cell line (HEK293FTs) takes place over 2-3 weeks. A triple transfection is performed to insert plasmids for the assembly helper, AAV capsid, and transgene of interest. After 3 d post-transfection, viral particles are retrieved by cell lysis and sequential purification steps. Titer range usually falls in the order of 10 ¹² vg per mL. Image courtesy of Alex N. Nazzari.	27
Figure 13	AAV vectors with a fluorescent reporter downstream of a translational control operator from the ATF4 5' UTR allow for the assessment of proteostasis dysfunction in neurons	29
Figure 14	(a) Suppression of reporter expression evaluated 48 h post-transfection. (b) Kinetic monitoring of expression stability over 20 h. (c) and (d) Induction of reporter expression following treatment with Thapsigargin (TG).	30
Figure 15	(A) Detection of ATF4 induction predominantly in glial cells following TM treatment. (B) Kinetic monitoring of number of cells exhibiting ATF4 induction over a period of 24 post-treatment. (C) Morphological changes concurrent with ATF4 induction.	31
Figure 16	Primary cortical neurons under normal culture conditions seven days after viral transduction. Stress-dependent expression (ATF4GFP, left,	32

arrow) is substantially lower than constitutively expressed GFP (cGFP, right)

- Figure 17 Primary neurons expressing cGFP (top) or ATF4GFP (bottom) untreated (left, control) or treated with TG for 24 h (right, +TG). Scale bar = 100 μ m. Population-based quantification of ATF4GFP induction from control following TG treatment. n > 3,000 neurons 33
- Figure 18 Representative images of primary neurons transduced with ATF4GFP (left) or cGFP (right) at 0 h and 20 h post-exposure to either the ER stress inducer TG (top) or DMSO control (bottom). Heatmap false coloring is used to represent GFP gray values for better visualization of fluorescent expression. Scale bar = 50 μ m 34
- Figure 19 Kinetic monitoring of ER stress in live neurons. (A) Kinetic plots for the mean ATF4GFP integrated intensity induction levels after TG (circles) or baseline levels with control (DMSO) treatment (squares) throughout the time-lapse imaging session. (B) Kinetic plots for the mean cGFP integrated intensity expression levels with TG (circles) or control (DMSO) treatments (squares). (C-D) Quantification of neurite area (neurite area = total area – cell body area) following TG-stress in either ATF4GFP or cGFP cultures. TG used at a final concentration of 100 nM. Error bars report SEM from biological triplicates. All kinetic plots are normalized to the initial reading to. 35
- Figure 20 Endpoint morphometric analysis of primary neurons following 48 h exposure to the ER stressor thapsigargin (TG). (A) Cortical neurons immunostained for β -tubulin III (TUJ1) to label projections. (B) and (C) Quantification of neurite branching and terminals as measured by the CellProfiler software. 36
- Figure 21 Illustration of the ubiquitin-proteasome system. Enzymatic labeling of proteins tagged for degradation with ubiquitin leads to the proteolytic processing through the proteasome complex to achieve protein degradation. 38
- Figure 22 Lentiviral vectors to express mutant α -synuclein A53T. (A) Linear vector map depicting a lentiviral backbone (LV) encoding for human α -synuclein A53T fused to mKate2 (red fluorescent protein). Expression is driven by the promoter eIF1 α . (B) Red fluorescence confirming the transduction capacity of LV- α -synuclein A53T in primary cultures at different multiplicities of infection (MOI). 40
- Figure 23 Phenotypic characterization of the effects of MG132 proteasome inhibition in primary neurons. (A) Dose-dependent decline in viable nuclei as determined by image analysis of DAPI staining. (B) Accumulation of ubiquitin positive inclusions. (C) Disrupted 45

expression pattern of the axonal protein tau following MG132 treatment. (D-F) Corresponding quantification based on n=4 biological replicates for each concentration.

- Figure 24 Population detection of cellular stress following proteasome inactivation. (A) Representative time-lapse microscopy images of $ATF4GFP$ induction in neurons after treatment with 10 nM of the proteasome inhibitor MG132. (B) Kinetic plot for the mean $ATF4GFP$ integrated intensity over the course of 40-h following MG132 treatment. Arrow indicate inflection point associated with cell loss. Error bars report SEM from biological triplicates. 46
- Figure 25 (A) Individual neurons from the same population show different rates of $ATF4GFP$ induction and time of cell death (loss of membrane integrity). Heatmap false coloring is used to represent GFP gray values for better visualization of fluorescent expression. Scale bar = 25 μm . (B) Intensity visualization plot for each neuron in (A) describing the intensity of $ATF4GFP$ expression at each time point. (C) Correlation plot between the time at which neurons showed maximum $ATF4GFP$ expression (left y-axis) and time of cell death (x axis). Percentage of total cell death for the corresponding time point (right y-axis). 47
- Figure 26 Formation of pathological tau following phosphatase inhibition in neurons. (A) Representative images showing phosphorylated tau (p-Tau) as detected by immunocytochemistry. (B) Image analysis revealed significantly higher total p-Tau puncta and (C) p-Tau area. 48
- Figure 27 Kinetic profile of neuronal stress following phosphatase inhibition. (A) Representative images from timelapse studies examining $ATF4GFP$ levels in primary cortical neurons treated with okadaic acid (OA). (B) Corresponding kinetic curves for two different doses of OA in neurons expressing either $ATF4GFP$ (top) or $cGFP$ (bottom). 49
- Figure 28 Induction of cellular stress in primary neurons at 10 d after the co-transduction with $ATF4GFP$ and mKate2-tagged α -syn(A53T) vectors. (B) Quantification of $ATF4GFP$ integrated intensity in neurons with (red) or without (blue) α -syn(A53T) expression. *** $p = 0.0002$ by two-tail Mann-Whitney test. 50
- Figure 29 (A) Representative time-lapse microscopy images from neurons expressing $ATF4GFP$ and left untreated (top) or subjected to α -syn(A53T) overexpression (bottom). (B) Neurons expressing $ATF4GFP$ and exposed to TG stress (top) or a combination of α -syn(A53T) and TG (bottom). Scale bar = 50 μm . (C) Corresponding kinetic plots for the mean $ATF4GFP$ integrated intensity for all groups. 53

Figure 30	Cellular health and aggregation following α -syn overexpression in neurons. (A) Assessment of cellular health via LDH quantification in cell media. Absorbance values are normalized to an untreated control. Multiple comparisons by Kruskal-Wallis test (untreated vs A53T+TG * $p = 0.0395$; rest not significant. (B) Quantification of mean α -syn(A53T) area (red fluorescence positive puncta) with (closed circles) or without (open circles) TG stress.	54
Figure 31	Constructs for the expression of the mesencephalic astrocyte-derived neurotrophic factor (MANF) either constitutively or ATF4-controlled.	57
Figure 32	Stress-dependent expression of MANF in N2a cells following treatment with thapsigargin (TG) for 24 h. (A) Representative microscopy images and (B) corresponding quantification of GFP intensity.	60
Figure 33	Timelapse monitoring of cell counts following exposure to the neurotoxin 6-hydroxydopamine (6OHDA). N2a cells were transfected with either cMANF, ATF4-MANF, ATF4-GFP, or cGFP and exposed to 200 or 80 μ M 6OHDA.	61
Figure 34	Algorithm for neurite analysis using CellProfiler	71

LIST OF SYMBOLS AND ABBREVIATIONS

6OHDA	6-hydroxydopamine
ATF (4, 5, 6)	Activating transcription factor-4, 5, 6
AAV	Adeno-associated viral vector
α -syn	Alpha-synuclein
SNCA	alpha-synuclein gene
AD	Alzheimer's Disease
bZip	Basic-leucine zipper domain
BiP	Binding immunoglobulin protein
CHOP	CCAAT-enhancer-binding protein homologous protein
CNS	Central nervous system
ER	Endoplasmic reticulum
EGFP	Enhanced green fluorescent protein
eIF2 α	Eukaryotic initiation factor 2 α
GRP78	Glucose-regulated protein 78
GFP	Green fluorescent protein
GADD34	Growth arrest and DNA damage-inducible protein
IRE1	Inositol-requiring enzyme 1
ISR	Integrated stress response
LDH	Lactate dehydrogenase
MANF	Mesencephalic astrocyte-derived neurotrophic factor
mRNA	Messenger RNA
MOI	Multiplicity of infection

OA Okadaic acid
uORF Upstream open reading frame
PD Parkinson's Disease
PERK Protein kinase RNA-like ER kinase
RNA Ribonucleic acid
TG Thapsigargin
TM Tunicamycin
UPR Unfolded protein response
5'UTR 5' untranslated region
vg/mL Viral genomes per milliliter
XBP1 X-box binding protein 1

SUMMARY

This work introduces a viral vector that captures intrinsic signals associated with the unfolded protein response (UPR) to control gene product delivery in neurons. The development of this molecular tool responds to the need for physiologically responsive gene therapy constructs to prevent unwanted side effects associated with the transgene overexpression. Additionally, when used as a reporter assay, this tool addresses a basic research need for the kinetic monitoring of cellular stress and proteostasis dysfunction in neurons. To address these needs, we designed a viral-based ATF4 reporter comprising 384 bp of the initial coding region, including the 5'UTR of human ATF4 as a translational control operator fused to an enhanced green fluorescent protein (EGFP). For biological characterization, we conducted extensive time-lapse fluorescent microscopy assays in several in vitro models of proteostasis dysfunction, including ER stress, proteasome inactivation, phosphatase inhibition, and alpha-synuclein overexpression.

CHAPTER 1. INTRODUCTION

1.1 Motivation

Neurodegenerative diseases are neurological conditions characterized by the progressive and severe loss of neurons leading to clinical symptoms such as cognitive impairment and motor dysfunction. The irreversible nature of these conditions gives rise to their often incapacitating and debilitating effects seen in patients.

The steady increase in life expectancy in the US has raised a call for immediate action in attending age-related diseases of which neurodegenerative diseases represent the most prevalent conditions¹. Major neurodegenerative disorders such as Alzheimer's Disease (AD) and Parkinson's Disease (PD) affect nearly 6 M patients in the US, predominantly over 65. The overall economic burden of PD, for example, is approximately \$51.9 billion² and, without therapies to stop disease progression, this burden is projected to increase³.

The study of human genetics combined with neuropathology have illuminated key mechanisms and features characterizing human neurodegenerative diseases. Consequently, a fundamental area of study has focused on how misfolded proteins and overall deficiencies in protein processing influence mechanisms of neurodegeneration. Hence, from a therapeutic point of view, misfolded protein assemblies and the mechanisms by which neurons process misfolded proteins have taken priority as viable targets for drug development⁴.

Amongst therapeutic drug prospects, biologics (cell, protein, or nucleic acid-based molecules) have drawn more attention due to their disease-modifying potential⁵. In

particular, gene therapies represent a rapidly emerging approach under consideration to effectively treat neurological disease. Based on current clinical trials, adeno-associated viral vectors (AAV) are the leading carriers for gene therapy in the CNS given their demonstrated stability and low immunogenicity⁶. This modality of gene therapy leverages the continued refinement of viral capsid engineering, which has yielded over a dozen different AAV serotypes with distinct targeting capacities, tropism, and ability to penetrate biological barriers such as the blood-brain barrier^{7,8}. Furthermore, by incorporating cell-specific promoters, AAVs allow for transcriptional targeting of specific cell populations⁹. Thus, AAV-based gene therapy could potentially modulate biological targets in brain structures with excellent specificity.

From a drug delivery perspective, several roadblocks in AAV-based gene therapy remain. Substantial effort is being put towards capsid engineering for predictable tropism and penetration of biological barriers⁷. At a cellular level, concerns persist over detrimental effects associated with sustained transgene expression, particularly when modulating dynamic biological pathways^{6,10-12}. For instance, AAV-mediated delivery of short-hairpin RNA, as well as green fluorescent protein (GFP) alone, can elicit significant toxicity in the CNS *in vivo*¹³. Moreover, heightened expression of potentially secreted therapeutic proteins (e.g., growth factors) in the CNS can lead to off-target side effects^{14,15}. Therefore, an AAV platform that would allow a degree of control over gene product output could maximize the potential for gene therapies in neurodegenerative diseases.

1.2 Dissertation structure

The overarching goal of this work was to design and characterize expression vectors that were responsive to physiological changes associated with neurodegenerative disease. To accomplish this, we adopted regulatory elements from the unfolded protein response (UPR), a homeostatic mechanism used by cells to cope with stress (discussed in **Chapter 2**). Thus, by harnessing a biological signal associated with how cells respond to stress conditions, we created stress-responsive viral vectors and demonstrated their use in neurons.

Chapter 3 describes the design and initial characterization in both human-derived cell lines and mouse primary neurons. **Chapter 4** provides an extensive validation of stress-dependent expression in neurons experiencing neurodegenerative-like conditions. **Chapter 5** summarizes an efficacy study examining expression vectors to deliver the mesencephalic astrocyte-derived neurotrophic factor (MANF) as a neuroprotective approach. In **Chapter 6**, we discuss the broader implications of the results presented in the preceding chapters, areas of improvement, and potential applications. Importantly, beyond the concept of stress-responsive gene therapy, we use these vectors as a biological tool to describe neuronal responses to proteostasis impairment in non-destructive cell-based assays. Collectively, this work represents an initial step towards assessing the feasibility of a physiologically responsive gene therapy based on cellular stress signaling.

CHAPTER 2. BACKGROUND

The protein homeostasis (proteostasis) network comprises the processes by which cells control protein production, maintenance, and degradation to support cellular function¹⁶. Maintaining proteostasis requires an intricate balance among essential functions, including protein biosynthesis and folding, as well as proteome stabilization, degradation, and conformational maintenance. Failure in any of the processes within the proteostasis network inevitably leads to proteostasis dysfunction. The byproduct of proteostasis dysfunction is the accumulation of misfolded proteins and organelle damage, further perpetuating a proteostasis dysfunction cycle.

The cellular response to proteostasis dysfunction aims to restore balance and alleviate proteotoxic burden^{17,18}. This chapter summarizes relevant literature about cellular responses to proteostasis dysfunction, emphasizing the PERK/ATF4 pathway of the unfolded protein response.

2.1 Cellular Responses to Proteostasis Dysfunction

2.1.1 *Introduction to the Unfolded Protein Response*

It is well established that biological systems maintain homeostasis through negative feedback control networks. To maintain proteostasis, the endoplasmic reticulum (ER) serves as an intracellular sensor that captures signals associated with proteostasis dysregulation and induces corrective measures through a series of signaling events collectively known as the unfolded protein response (UPR)¹⁹. The UPR in the ER is activated by ER stress – a biological consequence of the imbalance between proper protein

handling (i.e., folding, trafficking, degrading) and the cellular ER capacity. The UPR is broadly defined as part of the integrated stress response (ISR), which expands to stressors beyond the ER, such as amino acid deficiency, viral infection, and heme deprivation²⁰.

In the mammalian system, three signaling programs, or “arms”, govern the UPR and are mediated by protein kinase RNA-like ER kinase (PERK), activating transcription factor 6 (ATF6), and inositol-requiring enzyme 1 (IRE1), respectively. Conversely, in yeast, the UPR is known to be exclusively controlled by IRE1²¹. As illustrated in figure 1, each signaling program (PERK, IRE1, ATF6) evokes an adaptive transcriptional response to alleviate overwhelming cellular stress by combining corrective actions that include reducing protein synthesis, increasing protein folding machinery, and promoting clearance of misfolded proteins¹⁹.

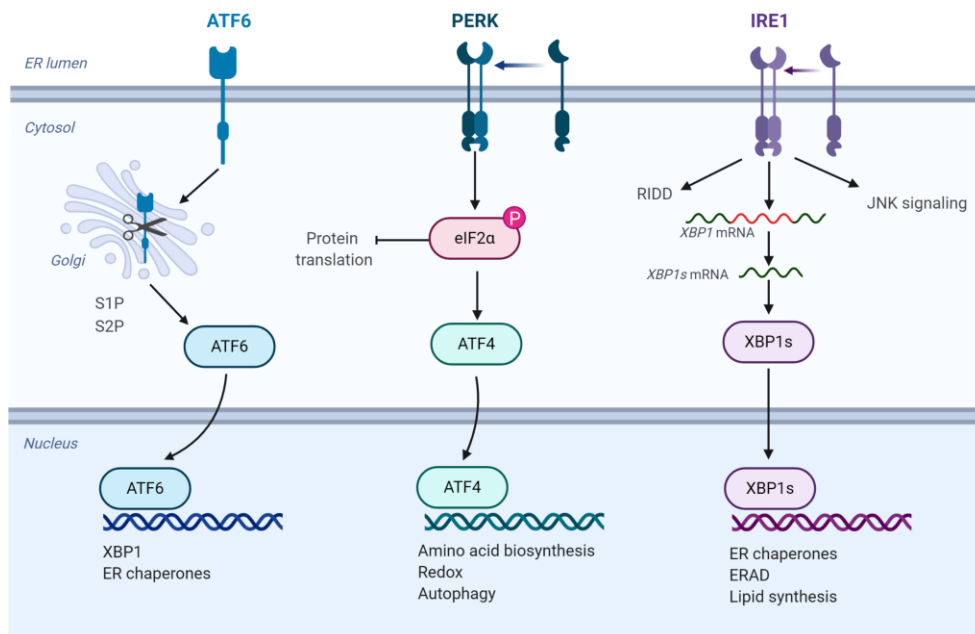


Figure 1: The unfolded protein response (UPR) is controlled by three transmembrane sensors in the ER. Activation of the ATF6 arm leads to the nuclear translocation of cleaved ATF6. Similarly, activation of PERK leads to a global halt in protein translation except for a select number of mRNAs such as *ATF4*. IRE1 arm exerts corrective functions via splicing of *XBPI* mRNA. Collectively, activation of the UPR leads to an overall increase in the cellular capacity to manage proteostasis. Created with BioRender.

The scientific consensus is that during this adaptive phase, the initial actions of the UPR are cytoprotective and proportional to the level of proteotoxic burden. For instance, during the early stages of the UPR, ATF6 signaling emphasizes protein refolding actions, whereas IRE1 acts later to trigger both refolding and protein degradation mechanisms²². However, upon unresolved cellular stress, the PERK arm of the UPR, in coordination with IRE1^{23,24}, activates a molecular switch to induce cell death via apoptosis, thereby preventing the presence of cells with unresolved stress to remain in an organism^{18,25}. In this scenario, the CCAAT-enhancer-binding protein homologous protein (CHOP), a downstream product of PERK, triggers cell death as an apoptotic gene²⁶. Notably, the

cytoprotective-to-apoptosis switch threshold varies across cell types, making the cellular fate upon UPR activation cell and context-dependent¹⁸.

While predominantly associated with proteostasis dysfunction, UPR activation has also been observed following injury²⁷, hypoxia²⁸, and inflammation²⁹. Important to note that in the context of neurodegeneration, optimal UPR signaling is also influenced by aging. Specifically, changes in UPR signaling during aging are attributed to reduced activity of the UPR sensor BiP³⁰ and other effectors³¹. Additionally, age-dependent oxidation has been shown to negatively impact chaperone capacity resulting in impaired corrective measures following UPR induction³². This collapse of efficient UPR engagement during aging results in the accumulation of misfolded proteins as well as in a diminished cellular capacity to overcome additional proteostasis burden³³.

2.2 The PERK Arm of the Unfolded Protein Response

2.2.1 Physiological Implications of PERK/ATF4 Signaling

Activation of the PERK arm of the UPR is mostly recognized for halting protein translation to alleviate the perceived burden to the proteostasis network. While conserved across mammalian species, together with ATF6, PERK control of the UPR is specific to mammalian cells³⁴. The physiological role of PERK is exemplified by data that suggest that PERK mutant cells are unable to establish an efficient UPR to cope and survive ER stress³⁵. Specifically, disrupting PERK activation hinders the recruitment of corrective measures induced by downstream effectors such as the eukaryotic initiation factor 2 α (eIF2 α)³⁶. PERK, therefore, serves an essential role in the ability of mammalian cells to respond and counteract proteostasis impairment.

2.2.2 Effector response by ATF4

The activating transcription factor 4 (ATF4) is a 351 amino acid protein member of the basic-leucine zipper (bZip) group of transcription factors. ATF4 mRNA is expressed ubiquitously across tissues; however, its level and degree of regulation are considered tissue specific⁴⁰. Mounting evidence strongly positions increased ATF4 levels as a biological signature in cells undergoing stress. The increased levels of ATF4 under stress conditions stem from both increased transcript levels as well as the preferential translation of ATF4 mRNA following PERK activation⁴¹.

At the mRNA level, the human ATF4 sequence is organized with several short upstream open reading frames (uORFs) in the 5' untranslated region (UTR) leader sequence, which precedes the protein's functional coding region⁴². During normal conditions, ribosome scanning starts downstream of uORF1, leading to the suppression of ATF4 expression after uORF2 scanning. In contrast, under conditions of stress, ribosome reinitiation proceeds downstream of uORF2, leading to the translation of ATF4 given the overlap with the ATF4 coding region⁴³.

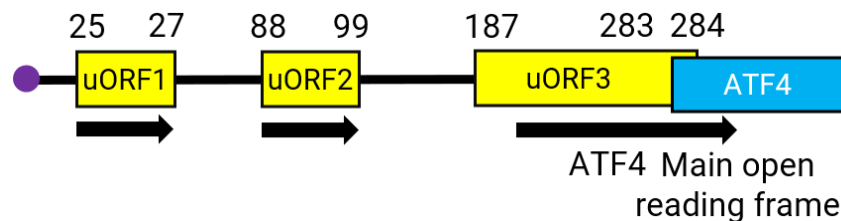


Figure 3: Human *ATF4* initial coding segment sequence including upstream open reading frames (uORFs) for stress-responsive translational control. Ribosome

scanning downstream of uORF2 leads to the translation of ATF4 given the overlap between ATF4 main open reading frame and uORF3.

ATF4 is considered an integral effector of the PERK arm of the UPR due to its preferential translation during UPR activation. Upon induction, ATF4 orchestrates a transcriptional program to establish an adaptive response (restore homeostasis) or a terminal response (trigger cell death). The dynamics of ATF4 and cellular fate relationships are summarized in figure 4. The severity and duration of stress determine which type of response predominates. To this purpose, ATF4 is regulated by GADD34 in a negative feedback control loop that attenuates ATF4 levels by deactivating eIF2 α ⁴⁴. Thus, the translational control of ATF4 can influence a myriad of cellular outcomes as mammalian cells cope with stress in a context-dependent manner.

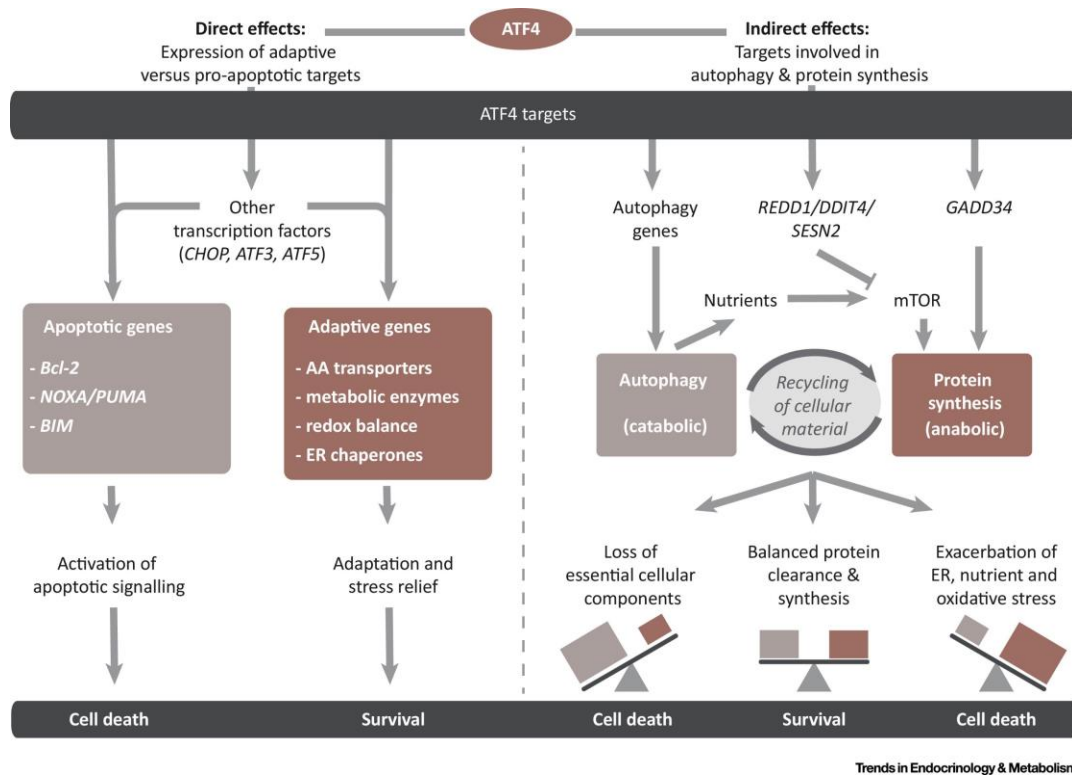


Figure 4: Downstream effects of ATF4 induction following activation of the unfolded protein response. Transcriptional programs led by ATF3, CHOP, and ATF5 control

cellular fate decisions such as death or survival. Indirect effects of ATF4 activity influence proteostasis functions such as protein degradation (autophagy) and protein synthesis rates. Adapted from ⁴⁵

2.2.3 *Relevance of PERK/ATF4 Signaling in Neurodegeneration*

Previous work implicates activation of the UPR and ER stress in a wide range of neurodegenerative conditions, including Parkinson's disease⁴⁶, Alzheimer's disease⁴⁷, amyotrophic lateral sclerosis⁴⁸, and Huntington's disease⁴⁹. Whether UPR activation is a causative factor for proteostasis dysfunction remains to be clarified. Nonetheless, mounting evidence suggests that PERK/ATF4 signaling is influenced by key factors associated with neurodegeneration such as aging, oxidative stress, and inflammation. This section will focus on Parkinson's disease (PD) to illustrate the relevance of PERK/ATF4 signaling in neurodegeneration.

PD is considered an *α -synucleinopathy*, a term used to describe the set of neurodegenerative diseases where the intracellular accumulation of the protein α -synuclein (α -syn) is regarded as a pathological hallmark. In addition to PD, major α -synucleinopathies include Dementia with Lewy Bodies (DLB) and Multiple Systems Atrophy (MSA). Each condition is strongly associated with the presence of cellular inclusions of toxic protein assemblies referred to as "Lewy pathology," of which α -syn is the main component^{50,51}.

Initial evidence of UPR activation in PD came from immunohistochemical examination of brain tissue from control subjects and PD patients⁴⁶. In this report, levels of active PERK (phospho-PERK) and active eIF2 α (phospho-eIF2 α) were substantially higher in the dopaminergic neurons of PD patients than control subjects. Immunoreactivity

for both phospho-PERK and phosphor-eIF2 α was remarkably higher in neurons with α -synuclein pathology.

Interestingly, a higher degree of PERK activation matched the early stages of the disease (~2-year duration of clinical PD) followed by more than a two-fold decline at later stages. While it is possible that disease pathophysiology can compromise UPR signaling, this decline, however, may also be due to the natural decrease in UPR activity associated with aging. Nonetheless, clinical data suggesting activation of UPR markers early in disease progression is further supported by *in vitro* studies where parkinsonian toxins induce PERK and eIF2 α activation before more detrimental processes like mitochondrial fragmentation and apoptosis⁵².

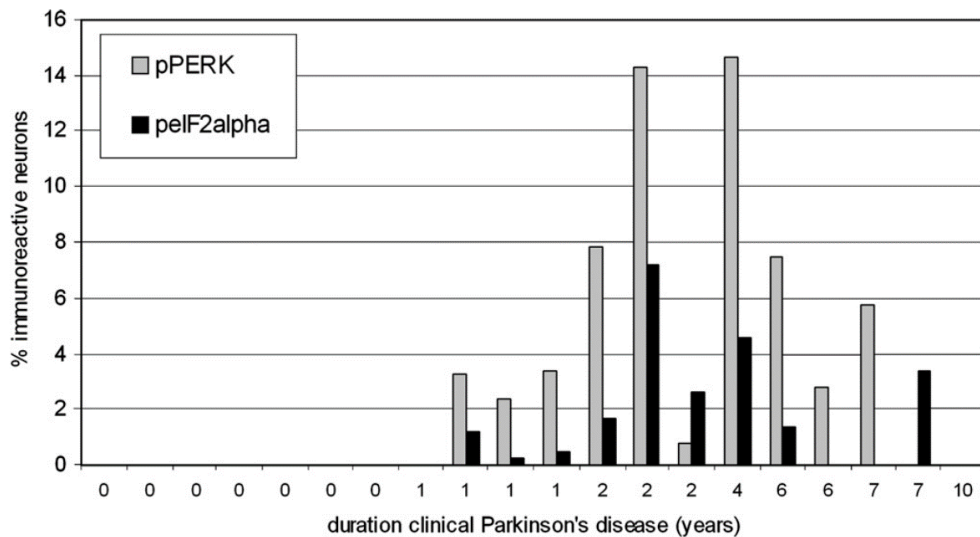


Figure 5: Immunohistochemical examination of markers for the PERK/ATF4 arm of the unfolded protein response (active PERK and eIF2 α) in tissue from patients with confirmed clinical Parkinson's Disease. Adapted from ⁴⁶

The relevance of the UPR in α -synucleinopathies is further exemplified by studies establishing that ER stress is a pathological signature of α -syn pathology in neurons⁵³,

which likely stems from the accumulation of α -syn in the ER over time^{54,55}. From a mechanistic point of view, it has been shown using SH-SY5Y cells that, upon misfolding, α -synuclein interacts with BiP to trigger PERK activation leading to increased ATF4 levels⁵⁶. Consistent with these findings, analysis of UPR activation in patient induced pluripotent stem cell-derived neurons with *SNCA* (α -synuclein) triplication show induction of all three branches of the UPR⁵⁷. As a mechanism of neurodegeneration, the ATF4 target gene *Trib3* has been identified as a key mediator of neuron death upon UPR activation in PD⁵⁸.

Whether UPR activation and increased ATF4 levels signify a detrimental or beneficial outcome for the cell remains unclear, although it appears context and time-dependent. For instance, AAV-mediated overexpression of ATF4 exacerbates α -syn-induced neurodegeneration in dopaminergic neurons⁵⁹. Consistent with these findings, inhibition of PERK/ATF4 signaling via small-molecule⁶⁰ or genetic methods⁶¹ proves sufficient to be neuroprotective in rodent models of PD. Divergent results, however, show that the expression of ATF4 is neuroprotective against neurotoxins that induce Parkinson-like symptoms⁶².

In conclusion, cellular responses to proteostasis dysfunction are driven by the UPR, which is recognized as a key cell-autonomous factor in PD. Moreover, expression of all major mediators of the PERK/eIF2 α /ATF4 pathway (i.e., p-PERK, p-eIF2 α , ATF4, CHOP, Trib3) has been detected in human brains affected by α -syn pathology⁵⁸⁻⁶¹. Mechanistically, cellular outcomes of sustained UPR activation such as apoptosis and diminished protein translation can contribute to neurodegeneration.

2.3 Experimental Modulation of PERK/ATF4 Signaling

2.3.1 Pharmacological modulation

Table 1 summarizes the diverse number of drugs that have been studied for their potency to cause ER stress, engage the UPR, and cause cellular responses that mimic global proteostasis dysfunction. The drugs tunicamycin and thapsigargin are arguably the most commonly used agents to induce robust ER stress *in vitro* and *in vivo*. Over 3,000 references in PubMed® make use of either drug for studies of cellular stress. This section presents a brief overview of their mechanisms of action as it pertains to ER stress and UPR activation.

Tunicamycin (structure shown in figure 6) is an antibiotic known to act as an N-glycosylation inhibitor, causing rapid and widespread UPR activation across organisms in a dose-dependent manner^{63,64}. It has been used as a tool to demonstrate the detrimental impact on ER stress and activation of the UPR on the developing brain when administered systemically⁶⁵. When injected locally in the adult brain, it can recapitulate features of Parkinson's Disease pathophysiology such as death of dopaminergic neurons, motor impairment, and astrogliosis⁶⁶. Beyond being considered a “classical” inducer of ER stress, additional studies in neuronal cultures have revealed tunicamycin's ability to exacerbate the accumulation of aggregation-prone proteins such as alpha-synuclein^{54,67}, and TDP-43⁶⁸.

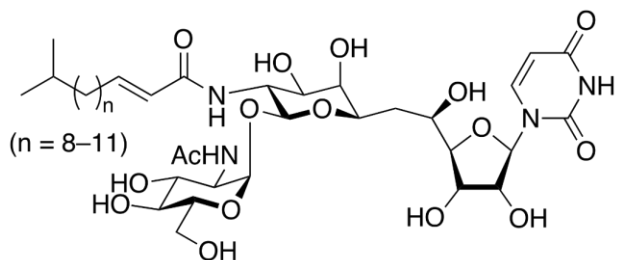


Figure 6: Tunicamycin (TM) structure. TM inhibits protein N-glycosylation in cells leading to accumulation of unfolded proteins in the ER and induction of the unfolded protein response. From Charley, Public Domain

Thapsigargin (structure shown in figure 7) is a lactone drug isolated from the plant *thapsia garganica* capable of penetrating biological membranes due to its excellent interactions with lipids. In cell and molecular biology research, thapsigargin is used a tool to induce swift calcium depletion from stored Ca^{2+} in the sarcoplasmic/endoplasmic reticulum Ca^{2+} -ATPase (SERCA). Disruption to Ca homeostasis by thapsigargin leads to ER stress, increased cytosolic Ca^{2+} , and UPR activation⁶⁹. Prior work suggests that the interplay between ER Ca^{2+} homeostasis and UPR activation is dictated by calcium-dependent protein folding enzymes and the Ca^{2+} buffering capacity of BiP/GRP78⁷⁰. Thus, by inhibiting SERCA function, thapsigargin disrupts ER function leading to proteostasis impairment and UPR induction.

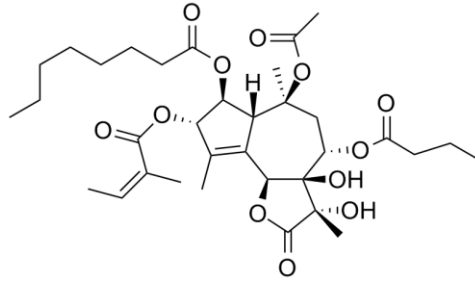


Figure 7: Thapsigargin (TG) structure. TG inhibits the SERCA pump creating a calcium imbalance which induces the unfolded protein response. From Charlesy, Public Domain

The cellular outcomes upon thapsigargin exposure are time and cell-type dependent. While the effects of thapsigargin on calcium levels are described to be fast (minutes) and transient⁷¹, cytotoxic effects are prominent upon long-term exposure (>12 h) to the drug or its analogs. Importantly, the detrimental outcomes are not specific to the cytosolic Ca²⁺ increase but depend on the degree to which SERCA Ca²⁺ depletion activates a sustained UPR⁷².

Pharmacological agents such as tunicamycin and thapsigargin are powerful tools to study stress signaling in cells because of their well-characterized mechanisms of action and temporal control over the induction of stress. Importantly, these inducers have broad capabilities in UPR activation, leading to increased signaling in all three branches. More recently, however, specific activators of PERK/ATF4 signaling have been described. For example, a small-molecule screen identified the compound CCT020312 to selectively activate PERK leading to eIF2 α phosphorylation in cancer cells while avoiding global UPR activation⁷³.

Table 1: Pharmacological modulators of the UPR in mammalian cells

Pharmacological agent	Description	Representative study
Tunicamycin	N-glycosylation inhibitor	65
Thapsigargin	SERCA inhibitor	72
DTT	Reducing agent	74
Okadaic acid	Phosphatase inhibitor	75
CCT020312	PERK activator	73
Salubrinal	eIF2 α activator	76
Sephin1	GADD34 inhibitor	77
GSK2606414	PERK inhibitor	78
MG132	Proteasome inhibition	79

2.3.2 Genetic modulation

The acute nature of global induction of ER stress and pleiotropic cellular responses unrelated to UPR signaling is a commonly recognized drawback of pharmacological inducers. To overcome these limitations, Bregmann et al. demonstrated that the expression of folding-defective polypeptides targeted to the ER activated a cellular response more attuned with UPR signaling than chemical inducers⁸⁰. This approach, however, lacks the temporal control of induction needed in most experimental designs. Improved methods, such as those inspired by chemical biology and chemogenetic manipulations could bridge the gap between specificity and feasibility to study UPR activation⁸¹.

2.4 Experimental Detection of PERK/ATF4 Signaling

2.4.1 Conventional molecular biology techniques

Commonly, the study of cellular responses to proteostasis dysfunction relies on the use of conventional molecular biology techniques such as western blot for protein quantification and quantitative polymerase chain reaction (qPCR) for gene expression analysis. Regularly used markers to study ER stress and UPR activation *in vitro* and *in vivo* include activated forms of PERK, IRE1, eIF2 α alone or in combination with downstream products such as ATF4, ATF3, spliced XBP1, or CHOP. These techniques are advantageous due to their well-established protocols and the ability to probe multiple markers from the same biological samples. However, biological insights derived from studying cellular stress using conventional molecular biology techniques are usually devoid of temporal and spatial resolution. As ensemble measurements, these techniques do not capture single-cell heterogeneity or individual cellular responses arising from a mixed cell population. Similarly, due to their destructive sample processing steps, the time-course evaluation of UPR induction is more challenging when examining precious or resource-intensive biological samples.

2.4.2 Fluorescent and luminescent reporters

Fluorescent and luminescent cell-based reporters are key tools to examine cellular signaling in live cells as they overcome many of the limitations posed by conventional molecular biology techniques. Direct measurement of UPR activation has been achieved using transcriptional or translational control constructs followed by a fluorescent or luminescent output signal (reviewed by Lajoie et. al⁸²). In mammalian systems, reporters

have been developed for all three signaling programs: IRE1, PERK, and ATF6. Additionally, reporter constructs for BiP, a protein acting upstream of PERK and IRE1, have also been introduced⁸³.

For IRE1 and PERK, reporter constructs harness the downstream molecular events of XBP1 splicing and ATF4 translation, respectively (Figure 8). On the other hand, BiP and ATF6 reporters have relied on transcriptional regulation, which yields stress response detection at a gene expression level.

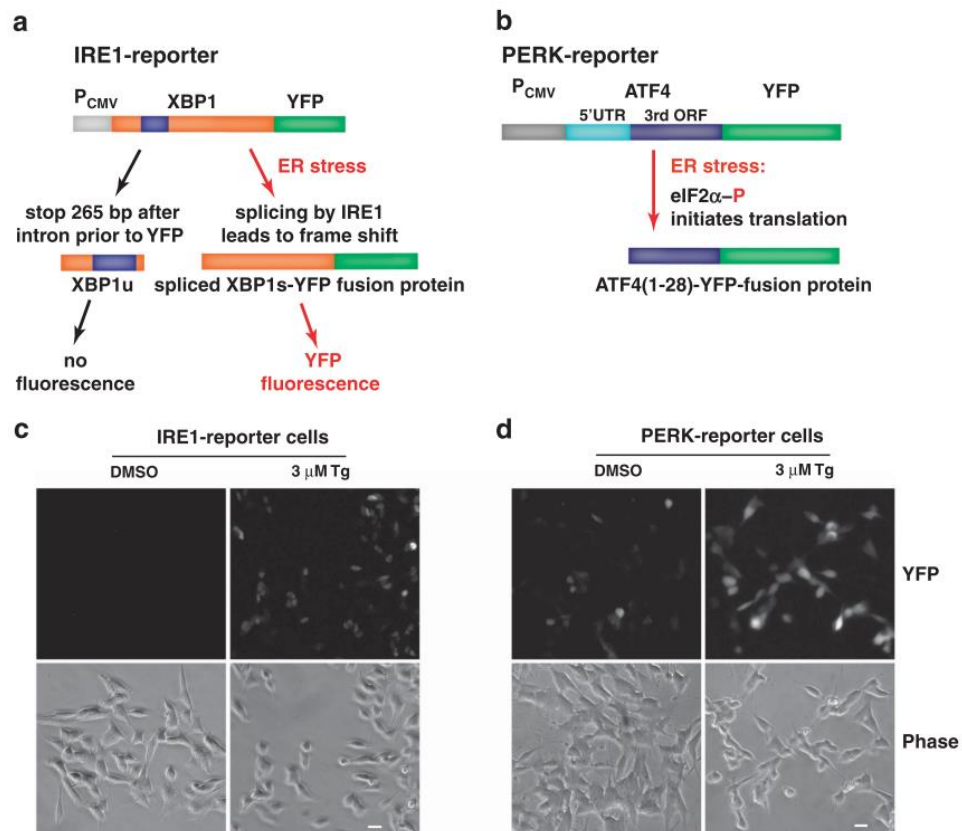


Figure 8: Cellular reporters of UPR activation via IRE1 or PERK signaling. (A) Selective XBP1 splicing upon UPR activation via IRE1 leads to a fluorescent readout.

(B) Selective translation of ATF4 following the phosphorylation of eIF2 α by PERK generates a PERK-based fluorescent readout. Adapted from ⁸⁴

Notably, the generation of UPR reporter constructs provides the advantage of generating reporter cell lines capable of providing insight into UPR activation in a non-invasive manner. For example, when combined with high-content imaging, specific UPR reporter cell lines have revealed the relative contributions and timing of each arm of the UPR concerning cellular fate^{24,25,84}. Furthermore, studies with UPR reporters have generated rich data sets for mathematical modeling of UPR regulation in mammalian cells^{83,85}. Collectively, reporter assays for UPR signaling represent a substantial improvement over conventional molecular biology techniques.

2.4.3 Transgenic mouse reporter lines

Closely based on their cell-based iterations, three examples of UPR stress reporters have been translated for use *in vivo*. The first report of fluorescent-based monitoring of the UPR and ER stress *in vivo* was based on IRE1 signaling⁸⁶. In this work, Iwawaki et. al developed a transgenic mouse line based on the splicing mechanism of XBP1. As demonstrated with IRE1 reporters *in vitro*, XBP1 splicing serves as a surrogate for IRE1 signaling activity after UPR induction. Following characterization with the ER stressors tunicamycin and thapsigargin, Iwawaki and colleagues demonstrated ER stress levels during different maturation stages across multiple tissues via *ex vivo* imaging (Figure 9). There are no derivative reports of this mouse line used in further research.

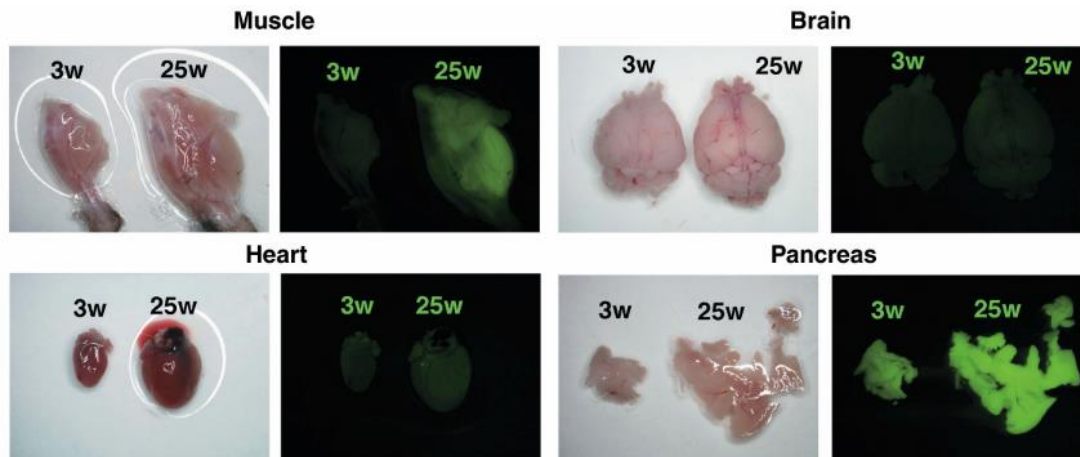


Figure 9: Application of an IRE1 reporter transgenic model to monitor UPR activation at different stages of development. Adapted from ⁸⁶

Recent efforts for monitoring ER stress *in vivo* have turned to reporter constructs based on ATF4 translational control and a luminescent output. Bioluminescent imaging of tissue extracted from ATF4 reporter transgenic mice subjected to tunicamycin-induced ER stress or amino acid deprivation revealed tissue-level heterogeneity in levels of cellular stress^{87,88}. Furthermore, when combined with a pharmacological model (carbon tetrachloride) of liver fibrosis, the ATF4-based transgenic model provided longitudinal measurements of ER stress in the liver (Figure 10).

Interestingly, besides a study in liver fibrosis, none of the UPR reporter mouse lines have been applied in disease-relevant contexts, nor have they demonstrated their feasibility to look at stress responses at a cellular level. Nonetheless, these studies validate that, in relevant physiological contexts, harnessing ATF4 translational control is a feasible approach to capture a biological signal associated with cellular stress.

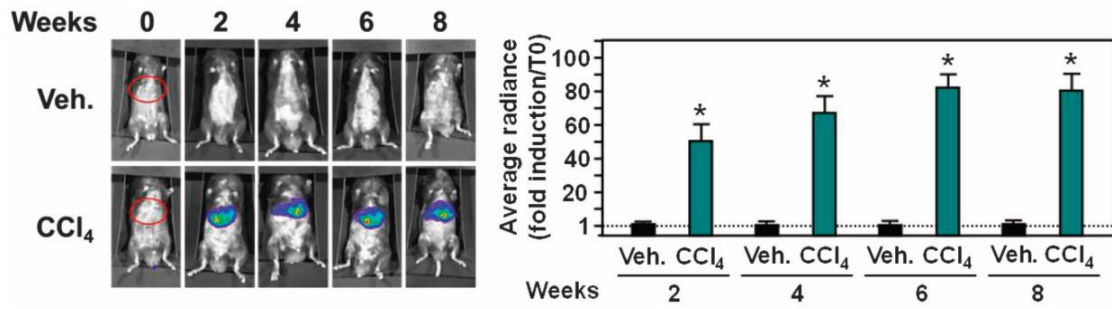


Figure 10: Application of a PERK/ATF4 reporter transgenic model to monitor UPR activation in a pharmacological model of liver fibrosis. Adapted from ⁸⁷

CHAPTER 3. Development and Characterization of Stress-Dependent Expression Vectors in Neurons

3.1 Introduction

Studies evaluating UPR activation have traditionally employed protein quantification methods for activated UPR kinases or mRNA quantification of UPR target genes such as ATF3 and Trib3. Notably, such conventional molecular biology methods have intrinsic limitations in assessing spatial and temporal profiles of cellular stress in live neuronal populations as well as limited resolution for discerning between individual cellular responses. The advent of reporter cell lines and luciferase-based stress reporters have enabled a more detailed study of the kinetic aspect of cell fate decisions during conditions of cellular stress⁸⁴. These tools, however, have not yet been adapted to neuronal systems. Neuronal models such as those established from primary sources better recapitulate neuronal physiology and function as they retain characteristics from their tissue of origin⁸⁹. However, primary neurons are generally challenging to transfect in sufficient numbers for high-throughput evaluation via fluorescence microscopy and are also vulnerable to assays requiring multistep cell culture manipulations. These limitations have collectively hindered progress to directly monitor and quantify the kinetics of stress responses in live neurons.

The work presented in this chapter describes the development and characterization of a viral-based reporter construct based on the 5' untranslated region (UTR) of the ATF4 ISR effector gene. By harnessing this selective translational event, we obtained a

quantifiable output following stress induction in primary mouse neurons. This chapter also describes how this reporter construct is incorporated in a cell-based assay to examine chronic stress responses evoked by pharmacological perturbation to the ER.

3.2 Methods

Cell culture

Human embryonic kidney (HEK) 293T cells were maintained in a humidified 5% CO₂ atmosphere at 37 °C in complete medium consisting of Dulbecco's Modified Eagle's medium (DMEM) supplemented with 10% fetal bovine serum, 2 mM L-glutamine, 100 international units (IU)/mL penicillin, and 100 µg/mL streptomycin.

Primary neuronal cultures

Flat bottom black 96 well plates (Greiner CELLSTAR®) were coated with fresh 100 µg/mL poly-L-lysine (Sigma) aqueous solution and incubated at 37 °C for at least 12 h. Coated wells were rinsed once with D-PBS and allowed to air dry for 2 h before use. Primary neurons were isolated from CD-1 E18 mouse embryos per approved protocols by the Emory University Institutional Animal Care and Use Committee, and National Institutes of Health guidelines. Brain cortices were dissected and dissociated using Worthington's Biochemical Papain Dissociation System (Worthington Biochemical Corporation) following the manufacturer's instructions and previously published protocols⁹⁰. Freshly dissociated neurons were plated in plating medium consisting of Neurobasal™ Plus base medium supplemented with 5% fetal bovine serum, 1 µg/mL gentamycin, and 2 mM Glutamax™-I (protocol is summarized in Figure 11). Complete

medium change was performed 12 h post-plating to maintenance medium consisting of Neurobasal™ Plus base medium supplemented with B-27 Plus, 2 mM Glutamax™-I, and 1% penicillin/streptomycin antibiotic cocktail (pen-strep). Partial medium changes were performed once a week after that with maintenance medium. Cortical neurons were considered mature and optimal for experiments at DIV 20-25.

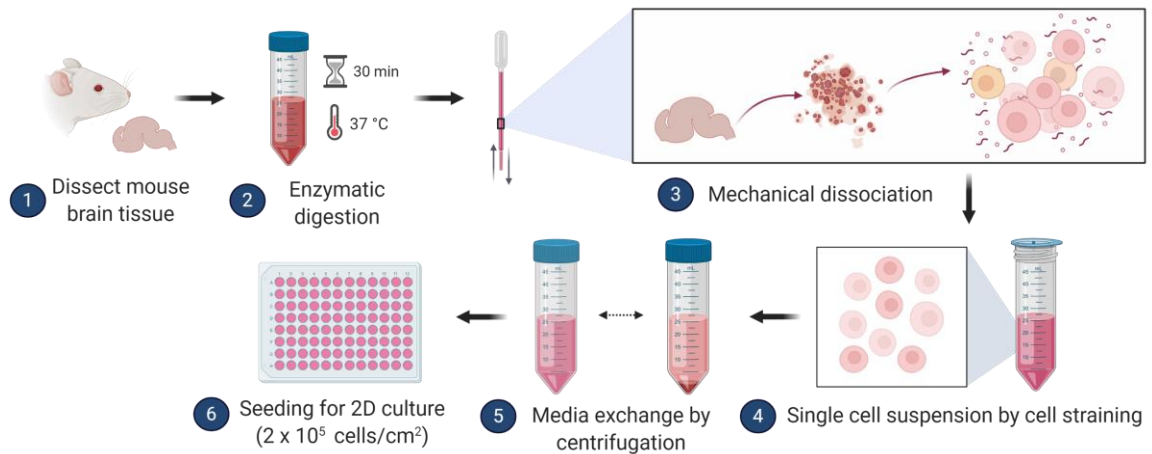


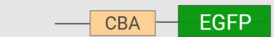
Figure 11: Summary of major steps in primary neuronal cultures. Dissected tissue is subjected to enzymatic digestion followed by mechanical dissociation. Cell suspension is cleared by cell straining and media exchange. Created by Angel Santiago-Lopez with BioRender.

Plasmid construction and vector production

To generate stress-dependent expression vectors, cDNA comprising 384 bp of the initial coding region including the 5'UTR of human ATF4 and flanked by the EcoRI and AgeI restriction sites was cloned into a pAAV-EGFP backbone plasmid using conventional molecular biology techniques. A similar construct lacking the ATF4 cassette was produced as a control for the constitutive expression of GFP. Transgene expression in both constructs is driven by the chicken β -actin (CBA) promoter for ubiquitous expression in mammalian cells. The correct sequences were confirmed by restriction enzyme digestion analyses and

DNA sequencing. Expression characteristics of each plasmid were evaluated in HEK 293T cells by transient transfection using Lipofectamine™ 3000 (Thermo Fisher Scientific). Expression vectors are further described in table 2.

Table 2: ATF4-based expression vectors

Construct linear map	Mode of expression	Abbreviation
	ATF4-controlled	_{ATF4} GFP
	constitutive	_c GFP

Adeno-associated viral vectors (AAV) of the DJ hybrid serotype were produced by following previously published protocols (refer to Figure 12)^{91,92}. Briefly, adherent HEK 293T cells were expanded and triple transfected with plasmids encoding for viral capsid, helper virus, and transgene of interest. After 3 d, cells were harvested and lysed by repeated freeze-thawing. Viral particles were purified by an iodixanol density gradient followed by buffer exchange and concentration in 100,000 MWCO filter units. Titer was determined by qPCR to be in the range of 10^{12} vg/mL

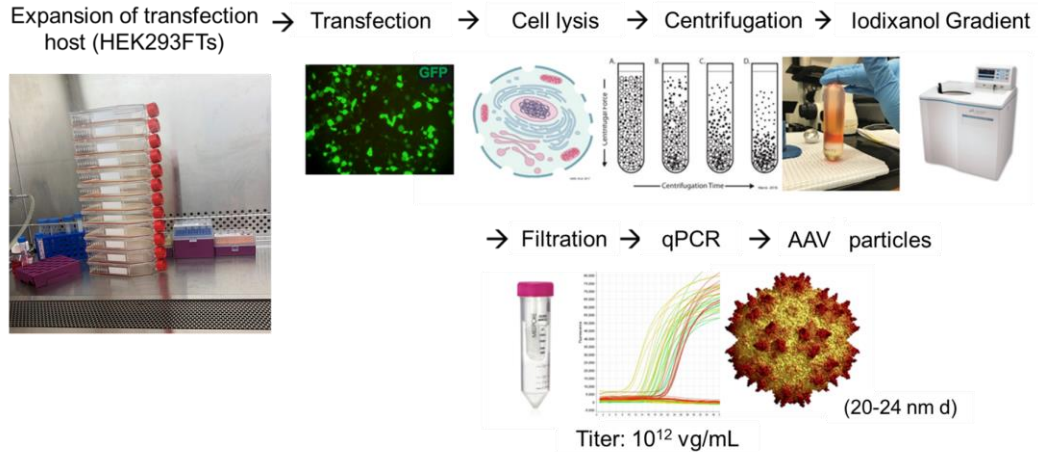


Figure 12: Process summary for the production of viral vectors. Expansion of the host cell line (HEK293FTs) takes place over 2-3 weeks. A triple transfection is performed to insert plasmids for the assembly helper, AAV capsid, and transgene of interest. After 3 d post-transfection, viral particles are retrieved by cell lysis and sequential purification steps. Titer range usually falls in the order of 10^{12} vg per mL. Image courtesy of Alex N. Nazzari.

Pharmacological treatments

Thapsigargin (Sigma) and Tunicamycin (Sigma) were solubilized in DMSO and working solutions were prepared in Neurobasal Plus/B-27 maintenance medium. From working solutions, drugs were added directly to the cells at the appropriate final concentration. Solvent-only solutions were used as the control for each drug, accordingly. The culture medium was not replaced after treatment to prevent additional disturbances.

Image acquisition and analysis

Live-cell imaging experiments were conducted using a Cytation 5 Cell Imaging Multi-Mode Reader (Biotek Inc.) equipped with a gas controller for CO₂ control and 4-zone temperature incubation with condensation control. Fluorescent images were acquired with either a 10X or 20X phase contrast objectives using either the DAPI, GFP, or CY5 built-in

LED filter cubes. The image acquisition routine was established in the Gen5 Plus software to follow a kinetic read taking at least 12 images in the same x- and y-coordinates for each well throughout the course of each time-lapse session.

Raw images were subjected to semi-automated pixel-based analysis using the Gen5 image analysis function. For reporter analysis, threshold settings were adjusted to capture GFP positive neurons. Image analysis metrics (GFP intensity, GFP area, and GFP integrated intensity) were calculated for each image in an experiment using the same threshold and masking settings. For neurite area quantification, phase-contrast images were analyzed to quantify cell body area, which was then subtracted from the total cell culture area. Calculated metrics were normalized to the corresponding first reading (t₀) to express a relative rate of change from baseline.

Immunocytochemistry

Primary neuronal cultures were fixed with 4% paraformaldehyde for 15 min and rinsed with PBS. Following permeabilization with 0.1% Triton X-100 for 5 min, cells were blocked with 4% normal serum for 30 min. Cultures were incubated overnight at 4 °C with primary antibodies followed by three rinses in PBS. Processed samples were incubated with appropriate secondary antibodies for 1 h at room temperature, counterstained with Hoechst 33342, and rinsed with PBS. The following antibodies were used: rabbit anti- β III tubulin (1:500, Abcam), and goat anti-rabbit Alexa Fluor® Plus 647 (1:1000, ThermoFisher Scientific).

3.3 Results

3.3.1 AAVs with ATF4-based translational control allow for stress-dependent transgene expression in neurons

The selective translation of ATF4 is a convergence point of the ISR following proteostasis dysfunction and activation of the UPR. To harness this event for enabling stress-dependent transgene expression in neurons (Figure 13), we first adapted ATF4 reporter by cloning the regulatory domain of *ATF4* including the 5'UTR and first 28 amino acids upstream of EGFP.

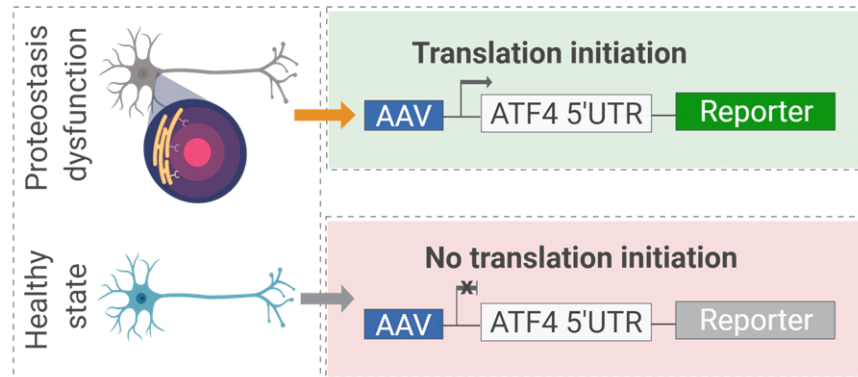


Figure 13: AAV vectors with a fluorescent reporter downstream of a translational control operator from the ATF4 5' UTR allow for the assessment of proteostasis dysfunction in neurons

Initial characterization of the resulting construct in HEK293 cells revealed stable reporter suppression following insertion of *ATF4* 5' UTR upstream of EGFP ($_{ATF4}GFP$) compared to constitutively expressed EGFP under the same promoter ($_cGFP$) (Figure 14A-B). Consistent with previous reports⁸⁴, induction of ER stress with thapsigargin (TG) in HEK293 cells led to a time-dependent increase in $_{ATF4}GFP$ expression intensity, and cell number (Figure 14C-D).

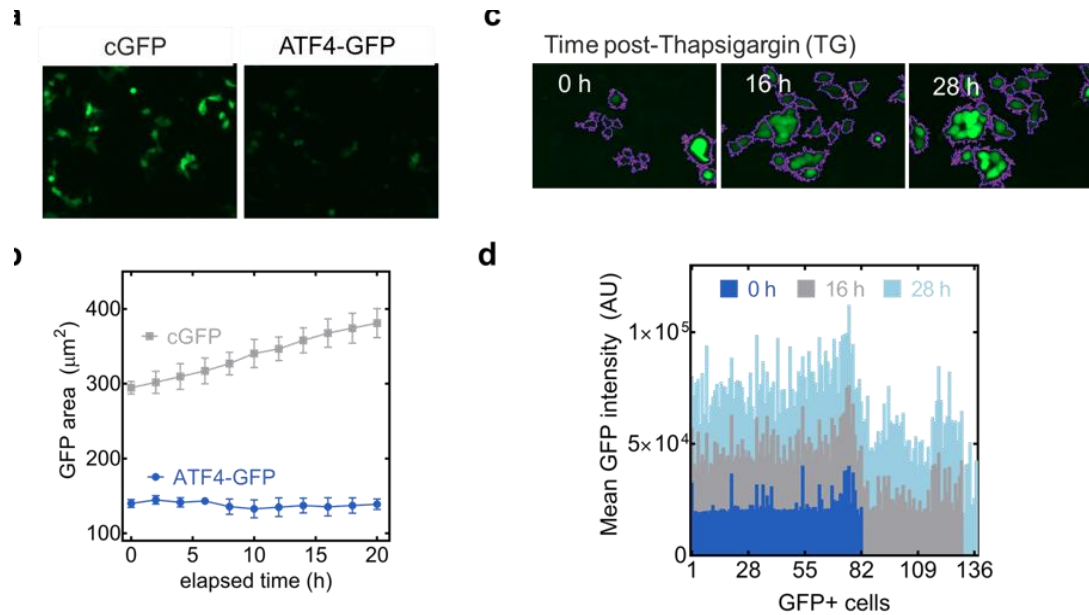


Figure 14: (a) Suppression of reporter expression evaluated 48 h post-transfection. (b) Kinetic monitoring of expression stability over 20 h. (c) and (d) Induction of reporter expression following treatment with Thapsigargin (TG).

Since conventional transfection methods are not compatible for high-throughput assessment of neuronal responses in sufficient numbers⁹³, we opted for AAVs as gene delivery vehicles. We first generated serotype 2 AAVs as this serotype is conventionally used for applications in neuroscience⁹⁴. Upon transduction of primary cultures and treatment with the ER stressor tunicamycin (TM), we observed a robust stress response that was captured by ATF4GFP as a fluorescent readout (Figure 15). This response, however, was attributed primarily to glial cells (presumably astrocytes).

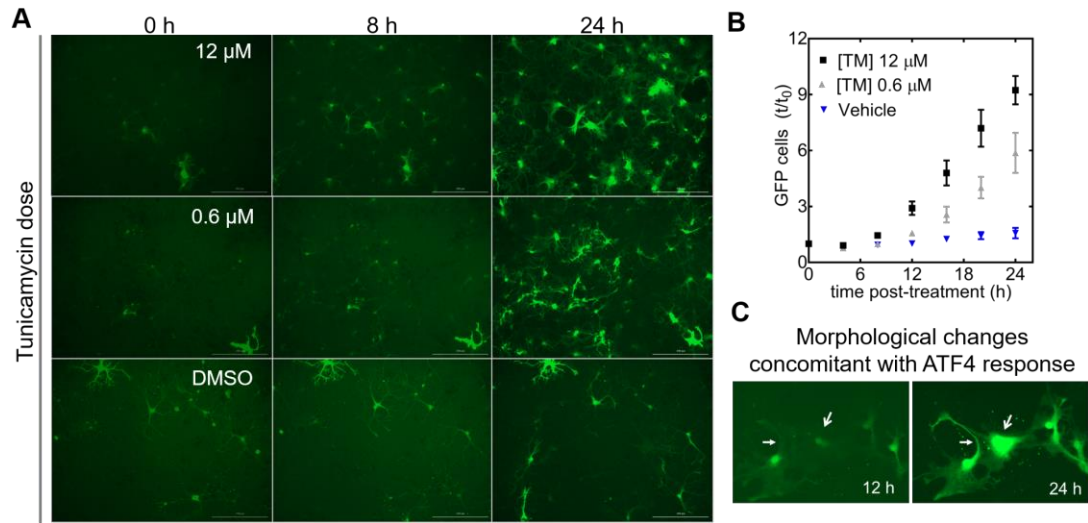


Figure 15: (A) Detection of ATF4 induction predominantly in glial cells following TM treatment. (B) Kinetic monitoring of number of cells exhibiting ATF4 induction over a period of 24 post-treatment. (C) Morphological changes concurrent with ATF4 induction.

The inability to capture stress responses in neurons led us to reexamine our choice of AAV serotype. While AAV2 is widely used in neuroscience and has been used historically in our lab, we noticed substantial differences when applied *in vivo* versus *in vitro*. Consequently, we turned our attention to AAVs with better performance in culture. We selected the DJ serotype (a hybrid capsid), which displays a superior transduction performance *in vitro* compared to other AAV variants⁹⁵. Similar to initial characterization in HEK293 cells, under standard culture conditions, primary cortical neurons transduced with AAV-DJ vectors carrying $_{ATF4}GFP$ showed suppression of reporter expression in neurons compared to cultures transduced with $_cGFP$ (Figure 16).

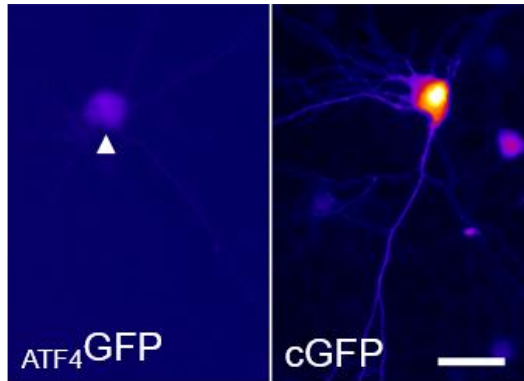


Figure 16: Primary cortical neurons under normal culture conditions seven days after viral transduction. Stress-dependent expression ($_{ATF4}GFP$, left, arrow) is substantially lower than constitutively expressed GFP ($cGFP$, right). Scale bar = 50 μm .

To evaluate the effectiveness of detecting stress response in neurons, we adopted TG, a classical inducer of UPR-ER stress, and previously used in our studies in HEK293s. TG typifies an ER-targeted pharmacological perturbation inhibiting the ER Ca^{2+} ATPase, causing ectopic calcium entry, ER stress, and eventually apoptosis⁶⁹. Upon 24 h exposure to 100 nM TG, cumulative distributions of cortical neurons transduced with $_{ATF4}GFP$ showed a rightward shift where >50% of the cell population showed at least a two-fold increase in mean $_{ATF4}GFP$ intensity compared to control cultures (Figure 17). Based on the degree of induction, these results suggest using $_{ATF4}GFP$ is an appropriate metric to capture stress responses in neurons.

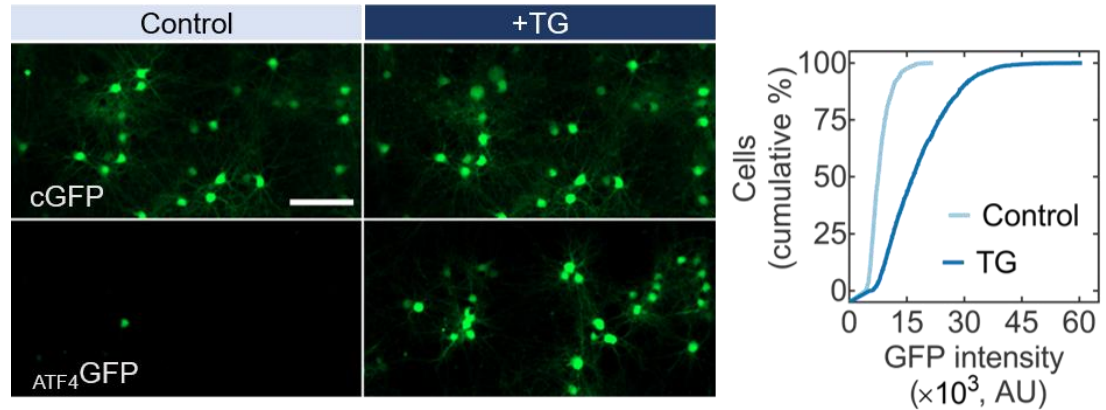


Figure 17: Primary neurons expressing cGFP (top) or $ATF4GFP$ (bottom) untreated (left, control) or treated with TG for 24 h (right, +TG). Scale bar = 100 μm . Population-based quantification of $ATF4GFP$ induction from control following TG treatment. $n > 3,000$ neurons

3.3.2 Kinetic monitoring of ER stress in neurons

Compared to other biological systems, the temporal analysis of stress responses from proteostasis dysfunction remains absent from the neuroscience literature. We first opted to characterize the kinetic profile of stress response in neurons exposed to TG in preparation for evaluating stress responses in more neurobiologically relevant contexts. Even though it is estimated that TG depletes stored Ca^{2+} in a timescale of minutes⁶⁹, chronic ER stress has been described to occur ~ 6 h post-addition of the ER stressor *in vitro*⁹⁶. We, therefore, designed live-cell imaging experiments to cover and exceed the time window for chronic ER stress responses. For the kinetic study of cellular stress in primary neurons, images were acquired every 2-3 h to prevent blue light-induced phototoxicity. Representative images at 0 h (baseline) and 20 h following treatment with TG of cortical neurons show a clear induction of $ATF4GFP$, primarily localized to the cell body (Figure 18, left panel). Neurons transduced with cGFP displayed comparable levels of expression with or in the absence of ER stress (Figure 18, right panel), as expected.

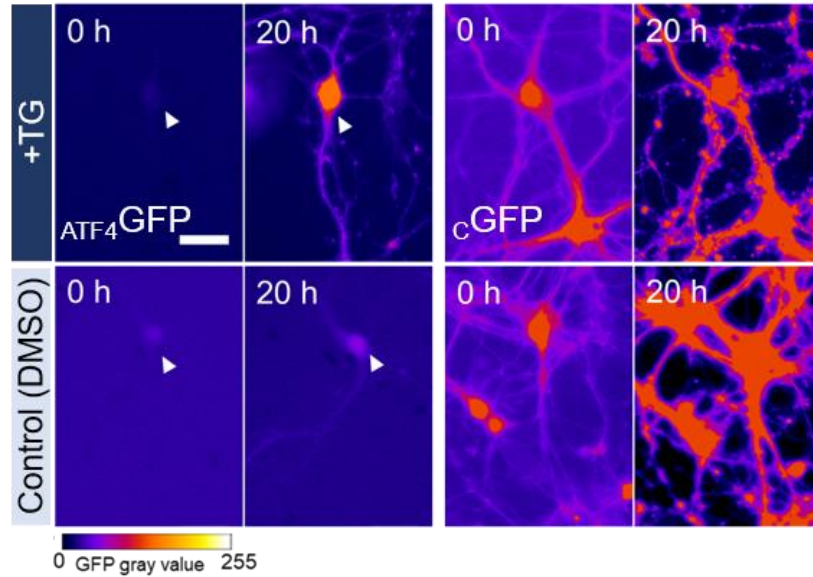


Figure 18: Representative images of primary neurons transduced with $ATF4GFP$ (left) or $cGFP$ (right) at 0 h and 20 h post-exposure to either the ER stress inducer TG (top) or DMSO control (bottom). Heatmap false coloring is used to represent GFP gray values for better visualization of fluorescent expression. Scale bar = 50 μm

The temporal profile of $ATF4GFP$ expression over 48 h revealed a three-fold induction in $ATF4GFP$ integrated intensity (the product of mean GFP intensity and area) compared to DMSO treated (control) cultures (Figure 19A). To ensure this rate of increase was a stress-dependent response, control neurons were transduced with $cGFP$ and subjected to the same experiment. Reflecting the lack of a stress-responsive element, neurons with $cGFP$ showed similar expression rates regardless of culture conditions over the 48-h period of experimentation (Figure 19B). Concomitant with ER stress, we found a time-dependent reduction (~20% total) in the neurite area consistent with a neurodegenerative-like manifestation of TG-induced ER stress in primary neurons (Figure 19C-D). A morphometric analysis of β -tubulin III stained projections confirmed the neurodegenerative-like effect of TG-induced ER stress across neurite metrics such as branching and terminal endpoints (Figure 20).

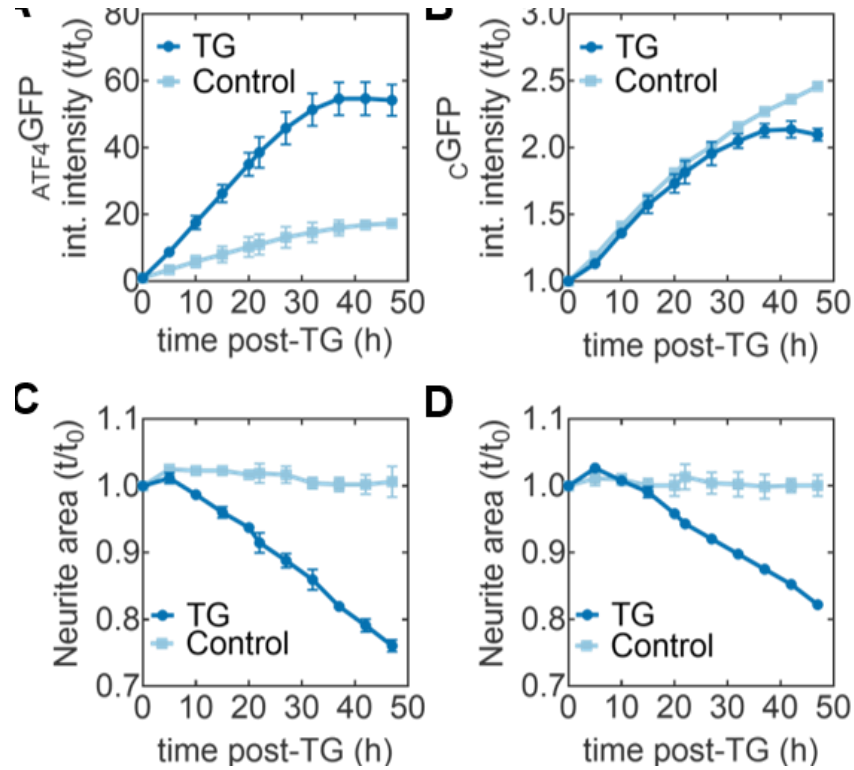


Figure 19: Kinetic monitoring of ER stress in live neurons. (A) Kinetic plots for the mean $ATF4GFP$ integrated intensity induction levels after TG (circles) or baseline levels with control (DMSO) treatment (squares) throughout the time-lapse imaging session. (B) Kinetic plots for the mean $cGFP$ integrated intensity expression levels with TG (circles) or control (DMSO) treatments (squares). (C-D) Quantification of neurite area (neurite area = total area – cell body area) following TG-stress in either $ATF4GFP$ or $cGFP$ cultures. TG used at a final concentration of 100 nM. Error bars report SEM from biological triplicates. All kinetic plots are normalized to the initial reading t_0 .

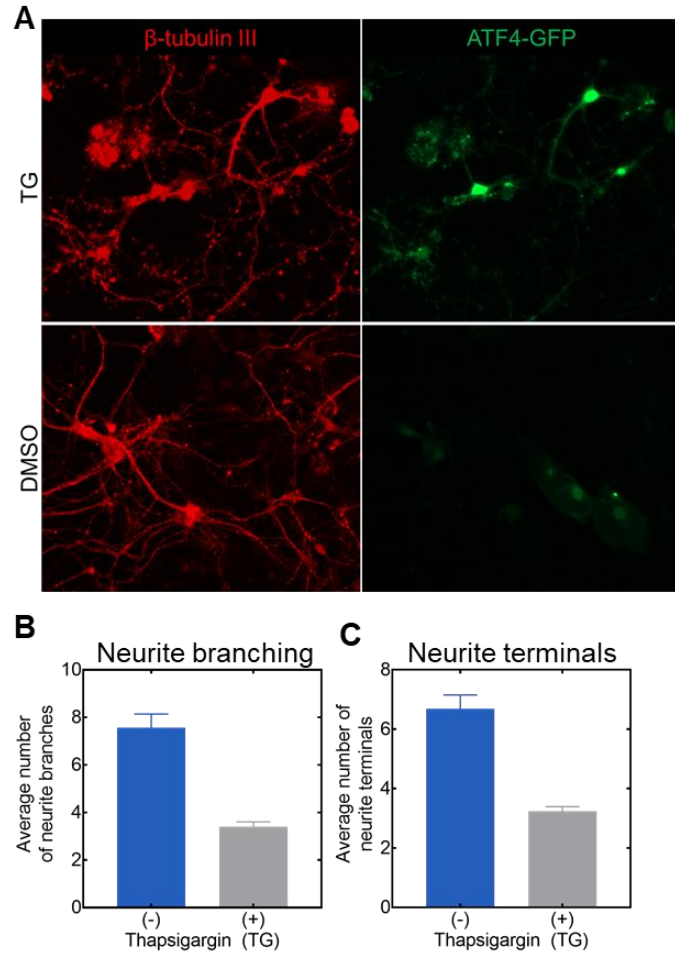


Figure 20: Endpoint morphometric analysis of primary neurons following 48 h exposure to the ER stressor thapsigargin (TG). (A) Cortical neurons immunostained for β -tubulin III (TUJ1) to label projections. (B) and (C) Quantification of neurite branching and terminals as measured by the CellProfiler software.

CHAPTER 4. KINETIC MONITORING OF NEURONAL STRESS IN MODELS OF PROTEOSTASIS IMPAIRMENT

4.1 Introduction

Proteostasis impairment results from an imbalance created when the function from one or more nodes of the proteostasis network is compromised. This imbalance elicits a condition of cellular stress, which triggers the mobilization of corrective processes led by the UPR signaling program. This chapter describes the application of stress-dependent expression vectors as a tool to examine UPR stress responses to proteostasis impairment in neurons. To this purpose, we implemented pharmacological and genetic manipulations to different nodes of the proteostasis network and monitored cellular stress over time. Each manipulation is described below.

Proteasome inhibition: Together with the autophagy-lysosomal pathway, the ubiquitin-proteasome system serves as a critical regulator of protein degradation to ensure proteostasis. Upon ubiquitin labeling, proteins tagged for degradation undergo proteolysis as they are transported through the proteasome complex⁹⁷ (Figure 21). Deficiencies in proteasome function are believed to contribute as a cell-autonomous factor driving neurodegeneration. For instance, Parkinson's patient-derived neurons display a global downregulation of proteasome function concomitant with heightened α -synuclein burden⁹⁸.

A diverse number of drugs with inhibitory activity over the proteolytic machinery of the proteasome have been developed to study the function of the ubiquitin proteasome

system. Clinically, many of these proteasome inhibitors have found applications in oncology⁹⁹. For research purposes, the drug MG132 (also termed Z-Leu-Leu-Leu-al) belongs to the peptide aldehyde class of proteasome inhibitors and remains one of the most widely used tools due to its potency and selectivity¹⁰⁰.

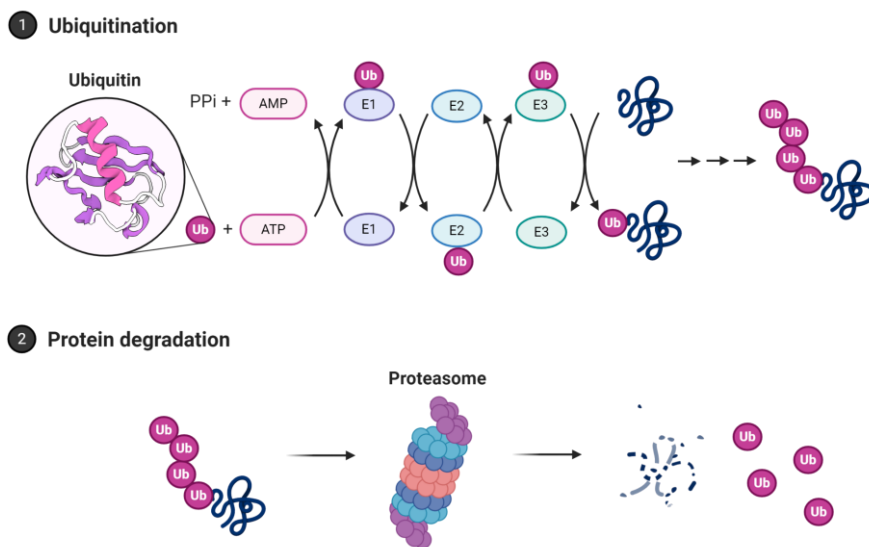


Figure 21: Illustration of the ubiquitin-proteasome system. Enzymatic labeling of proteins tagged for degradation with ubiquitin leads to the proteolytic processing through the proteasome complex to achieve protein degradation.

Phosphatase inhibition: The regulation of post-translational modifications in proteins influences proteostasis by ensuring proper protein conformational stability. Consequently, aberrant phosphatase activity has been implicated in the pathophysiology of neurodegenerative conditions like Alzheimer’s disease (AD). In AD, diminished phosphatase activity leads to the hyperphosphorylation of tau, a microtubule-associated protein in neurons, and the formation of neurofibrillary tangles, which are considered neuropathological hallmarks of neurodegeneration¹⁰¹. Okadaic acid (OA), potently inhibits the protein phosphatases PP2A/PP1 causing tau hyperphosphorylation, microtubule disassembly, cellular stress, and cell death^{102–104}. Hence, pharmacological approaches to

downregulate phosphatase activity such as OA have been adopted as non-genetic alternatives to AD modeling *in vitro* and *in vivo*¹⁰⁵.

A53T mutant α -synuclein overexpression: The protein α -synuclein (α -syn) is a relatively small protein (14 kDa) which predominantly exists as an unfolded monomer, although tetrameric conformations have been identified¹⁰⁶. The central region of the α -syn sequence (61-95 amino acids), initially described as the non-amyloid β component (NAC) of Alzheimer's plaques¹⁰⁷, is highly amyloidogenic and has been implicated in α -syn's aggregation-prone behavior^{108,109}. The physiological role of α -syn remains to be fully elucidated, but the consensus is that it takes part in neuronal communication as a structural component of presynaptic vesicles. However, human genetic studies have identified six mutations in the gene encoding α -syn (*SNCA*) to be linked to familial forms PD, alluding to the notion that α -syn has a causative role in the pathogenesis of the disease^{110,111}. Moreover, duplication or triplication of the *SNCA* gene can trigger early-onset PD, supporting the pathogenic role of α -syn even in its wild-type form. Notably, the A53T mutation influences α -syn aggregation propensity and severity of human PD. Even though not considered an ER protein, in rodent models, α -synuclein overexpression has been found to accumulate in the ER and disrupt ER signaling^{54,112}. We, therefore, opted for a lentiviral expression platform to establish the overexpression of α -syn(A53T) in neurons (Figure 22).

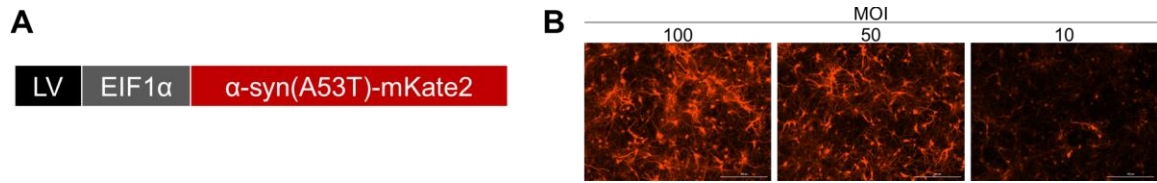


Figure 22: Lentiviral vectors to express mutant α -synuclein A53T. (A) Linear vector map depicting a lentiviral backbone (LV) encoding for human α -synuclein A53T fused to mKate2 (red fluorescent protein). Expression is driven by the promoter eIF1 α . (B) Red fluorescence confirming the transduction capacity of LV- α -synuclein A53T in primary cultures at different multiplicities of infection (MOI).

4.2 Methods

Primary neuronal cultures

Flat bottom black 96 well plates (Greiner CELLSTAR®) were coated with fresh 100 μ g/mL poly-L-lysine (Sigma) aqueous solution and incubated at 37 °C for at least 12 h. Coated wells were rinsed once with D-PBS and allowed to air dry for 2 h prior to use. Primary neurons were isolated from CD-1 E18 mouse embryos per approved protocols by the Emory University Institutional Animal Care and Use Committee and National Institutes of Health guidelines. Brain cortices were dissected and dissociated using Worthington’s Biochemical Papain Dissociation System (Worthington Biochemical Corporation) following the manufacturer’s instructions and previously published protocols ¹¹³. Freshly dissociated neurons were plated in plating medium consisting of Neurobasal™ Plus base medium supplemented with 5% fetal bovine serum, 1 μ g/mL gentamycin, and 2 mM Glutamax™-I. Complete medium change was performed 12 h post-plating to maintenance medium consisting of Neurobasal™ Plus base medium supplemented with B-27 Plus, 2 mM Glutamax™-I, and 1% penicillin/streptomycin antibiotic cocktail (pen-strep). Partial

medium changes were performed once a week thereafter with maintenance medium. Cortical neurons were considered mature and optimal for experiments at DIV 20-25.

Plasmid construction and vector production

To generate stress-dependent expression vectors, cDNA comprising 384 bp of the initial coding region including the 5'UTR of human *ATF4* and flanked by the *EcoRI* and *AgeI* restriction sites was cloned into a pAAV-EGFP backbone plasmid using conventional molecular biology techniques. A similar construct lacking the ATF4 cassette was produced as a control for the constitutive expression of GFP. Transgene expression in both constructs is driven by the chicken β -actin (CBA) promoter for ubiquitous expression in mammalian cells.

Adeno-associated viral vectors (AAV) of the DJ hybrid serotype were produced by following previously published protocols^{91,92}. Briefly, adherent HEK 293T cells were expanded and triple transfected with plasmids encoding for viral capsid, helper virus, and transgene of interest. After 3 d, cells were harvested and lysed by repeated freeze-thawing. Viral particles were purified by an iodixanol density gradient followed by buffer exchange and concentration in 100,000 MWCO filter units. Titer was determined by qPCR to be in the range of 10^{12} vg/mL.

For α -synuclein overexpression studies, lentivirus expression vectors encoding human A53T mutant α -synuclein fused to the red fluorescent protein mKate2 driven by the eIF1 α promoter were manufactured by VectorBuilder Inc. and reported to have a titer of 10^{12} vg/mL.

Pharmacological treatments

Thapsigargin (Sigma) was solubilized in DMSO, and working solutions were prepared in Neurobasal Plus/B-27 maintenance medium. MG132 (Abcam) and okadaic acid (Cayman Chemical) were handled in a similar fashion. From working solutions, drugs were added directly to the cells at the appropriate final concentration, as further described in the results section. Solvent-only solutions were used as the control for each drug, accordingly. The culture medium was not replaced after treatment to prevent additional disturbances.

Image acquisition and analysis

Live-cell imaging experiments were conducted using a Cytation 5 Cell Imaging Multi-Mode Reader (Biotek Inc.) equipped with a gas controller for CO₂ control and 4-zone temperature incubation with condensation control. Fluorescent images were acquired with either a 10X or 20X phase contrast objectives using either the DAPI, GFP, or CY5 built-in LED filter cubes. The image acquisition routine was established in the Gen5 Plus software to follow a kinetic read taking at least 12 images in the same x- and y-coordinates for each well throughout the course of each time-lapse session.

Raw images were subjected to semi-automated pixel-based analysis using the Gen5 image analysis function. For reporter analysis, threshold settings were adjusted to capture GFP positive neurons. Image analysis metrics (GFP intensity, GFP area, and GFP integrated intensity) were calculated for each image in an experiment using the same threshold and masking settings. For neurite area quantification, phase-contrast images were analyzed to quantify cell body area, which was then subtracted from the total cell culture area.

Calculated metrics were normalized to the correspondent first reading (t_0) to express a relative rate of change from baseline.

Immunocytochemistry

Primary neuronal cultures were fixed with 4% paraformaldehyde for 15 min and rinsed with PBS. Following permeabilization with 0.1% Triton X-100 for 5 min, cells were blocked with 4% normal serum for 30 min. Cultures were incubated overnight at 4 °C with primary antibodies followed by three rinses in PBS. Processed samples were incubated with appropriate secondary antibodies for 1 h at room temperature, counterstained with Hoechst 33342, and rinsed with PBS. The following antibodies were used: mouse anti-phospho-Tau AT8 (1:400, ThermoFisher Scientific), rabbit anti-ubiquitin (1:500, Agilent Dako), and donkey anti-mouse or goat anti-rabbit Alexa Fluor® Plus 647 (1:1000, ThermoFisher Scientific).

Lactate dehydrogenase (LDH) measurement

Lactate dehydrogenase (LDH) release was measured by using the CyQUANT LDH Cytotoxicity Assay (ThermoFisher Scientific) on collected cell culture supernatant according to the manufacturer's instructions. Absorbance was measured at 490 nm and 680 nm using the Cytation 5 plate-reader function. Results are reported as 680 nm-corrected absorbance normalized to untreated control cultures.

Statistics

Statistical analysis was performed in Graph Pad Prism 7. Data sets were tested for normality using the D'Agostino and Pearson test. For population comparisons not

following a normal distribution, statistics were calculated using a two-tailed non-parametric Mann-Whitney test. Multiple group comparisons were analyzed by the Kruskal-Wallis test. Results are reported as mean \pm SEM.

4.3 Results

4.3.1 Neuronal stress response to proteasome inactivation

A fundamental notion of the UPR is that in conditions of unresolved stress, this homeostatic mechanism switches into a terminal cell death signaling program³⁴. We combined live-cell imaging with global inactivation of the proteasome by MG132 to gain a more in-depth insight into the relationship between the temporal characteristics of the neuronal stress response and cell death. Additionally, employing a pharmacological inhibitor of proteasome function allowed us to probe neuronal stress in a condition of proteostasis impairment not directly related to ER-targeted perturbations such as TG. Importantly, proteasome impairment by cell-autonomous factors (e.g., protein oligomers) or disease co-factors (e.g., aging) has been implicated in the pathophysiology of several neurodegenerative disorders¹¹⁴. Specifically, proteasome inactivation by MG132 has been shown to activate PERK in primary neurons and Neuro-2a cells consistent with ER stress and UPR activation⁷⁹.

In primary cortical neurons, phenotypic characterization via immunocytochemistry following 24-h exposure to MG132 confirmed a dose-dependent decline in cell viability as well as an increase in ubiquitin-positive staining (Figure 23A-B, 23D-E). We additionally quantified the effect of proteasome inactivation on tau, a neuronal protein client of the proteasome¹¹⁵. We found a dose-dependent disruption in tau processing leading to a shift

from smooth to a punctate expression pattern (Figure 23C, 23F). Based on these results, we selected 100 nM as a working concentration to evaluate neuronal stress responses to proteasome inhibition within the time window of chronic ER stress.

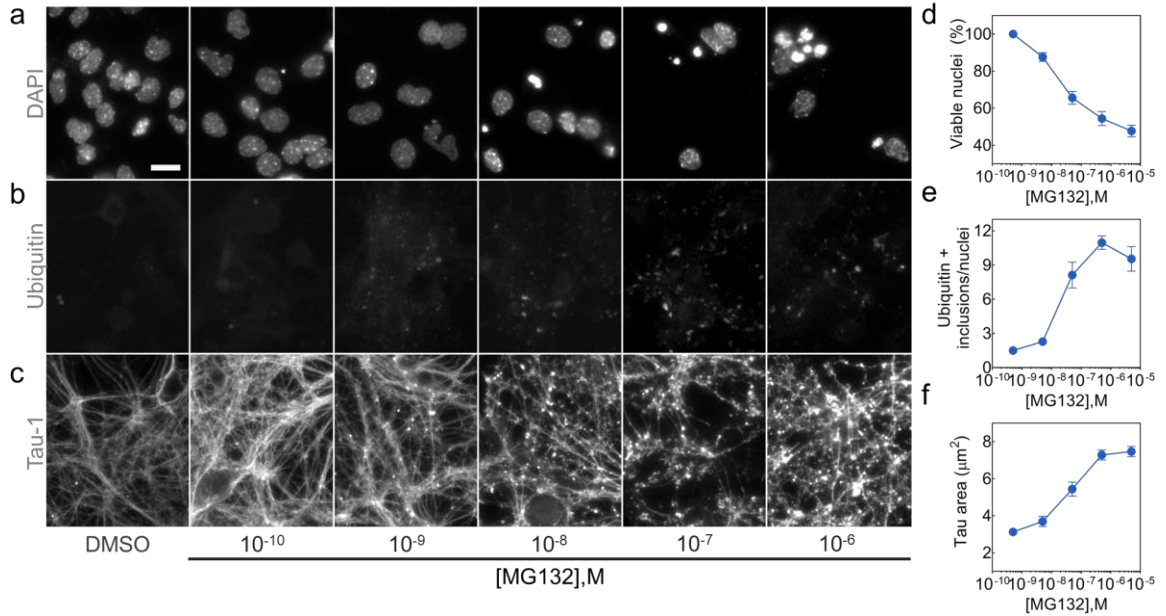


Figure 23: Phenotypic characterization of the effects of MG132 proteasome inhibition in primary neurons. (A) Dose-dependent decline in viable nuclei as determined by image analysis of DAPI staining. (B) Accumulation of ubiquitin positive inclusions. (C) Disrupted expression pattern of the axonal protein tau following MG132 treatment. (D-F) Corresponding quantification based on n=4 biological replicates for each concentration.

Upon treatment, we found that exposure to MG132 caused a robust increase in $ATF4$ GFP in neurons that peaked at 26-h post-treatment, followed by a signal decline associated with cell loss (Figure 24).

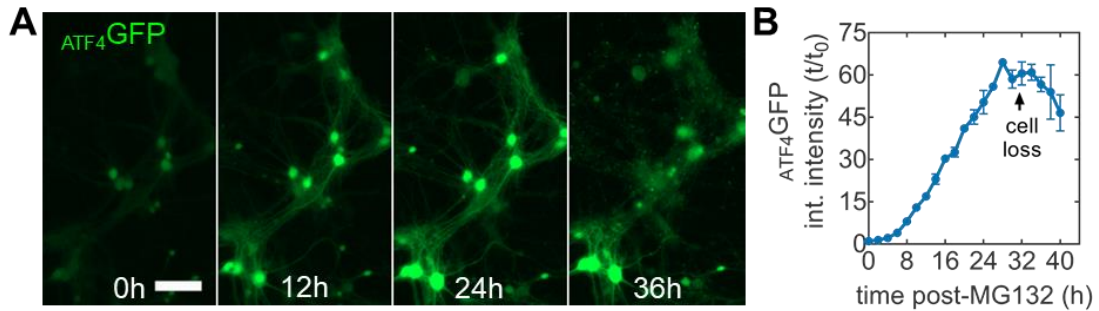


Figure 24: Population detection of cellular stress following proteasome inactivation. (A) Representative time-lapse microscopy images of $ATF4GFP$ induction in neurons after treatment with 10 nM of the proteasome inhibitor MG132. (B) Kinetic plot for the mean $ATF4GFP$ integrated intensity over the course of 40-h following MG132 treatment. Arrow indicate inflection point associated with cell loss. Error bars report SEM from biological triplicates.

UPR induction in neurons has been frequently described at a population level. However, a fundamental concept in cell biology is that individual members of a cell population can exhibit distinct biological responses¹¹⁶. We leveraged the capability of probing UPR-related stress responses by live-cell microscopy to visualize individual neuronal responses to proteasome inactivation by MG132. While the typical response, where an increase in $ATF4GFP$ was followed by loss of membrane integrity (cell loss), was consistent across the analyzed cells from the same population, the time of induction and cell death differed between individual neurons (Figure 25A). We found that delayed stress induction coincided with a later time of cell loss (Figure 25B), with ~54% of surveyed neurons dying between 34 and 40 h post-MG132 exposure. Furthermore, time point mapping of the time where $ATF4GFP$ is maximum versus time of cell loss showed a direct positive correlation (Figure 25C). Our analysis supports the notion that the time for each neuron to reach maximum $ATF4GFP$ expression can predict neuronal death asynchronism induced by proteasome inactivation.

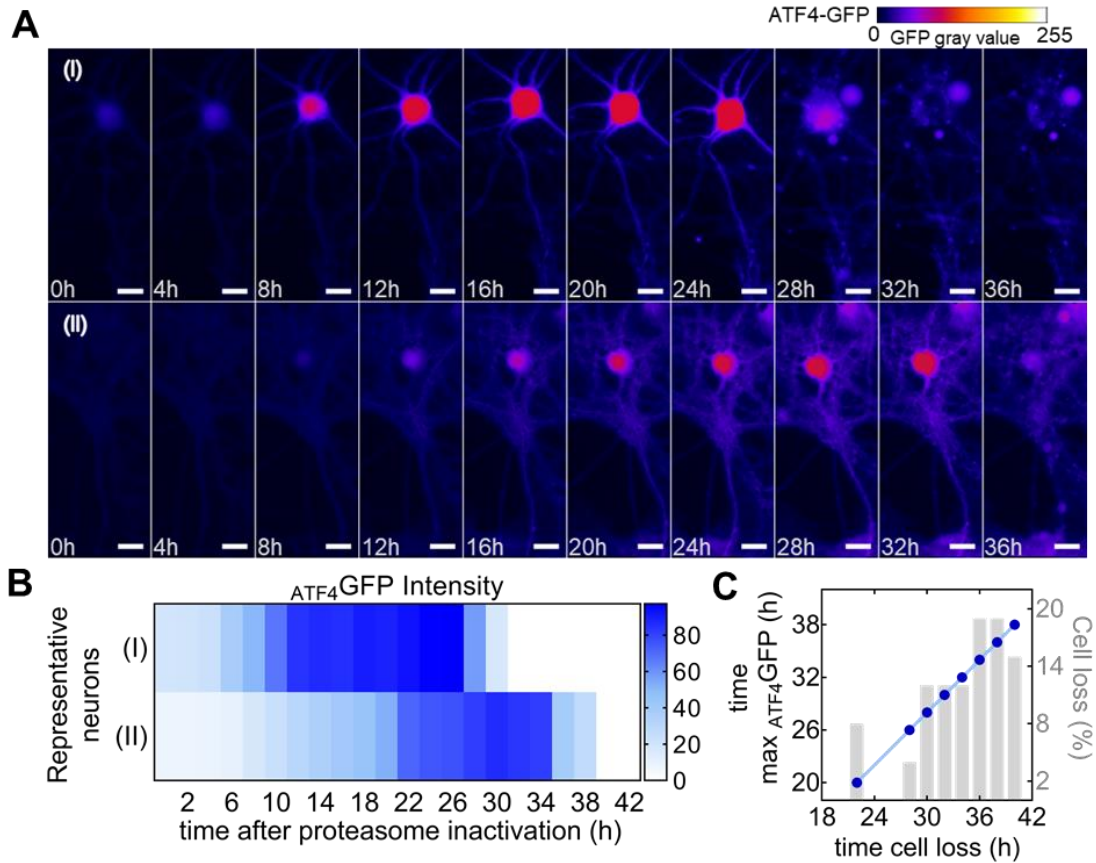


Figure 25: (A) Individual neurons from the same population show different rates of ATF4GFP induction and time of cell death (loss of membrane integrity). Heatmap false coloring is used to represent GFP gray values for better visualization of fluorescent expression. Scale bar = 25 μ m. (B) Intensity visualization plot for each neuron in (A) describing the intensity of ATF4GFP expression at each time point. (C) Correlation plot between the time at which neurons showed maximum ATF4GFP expression (left y-axis) and time of cell death (x axis). Percentage of total cell death for the corresponding time point (right y-axis).

4.3.2 Neuronal stress response to phosphatase inhibition

Okadaic acid (OA) PP1/2a inhibition leads to pSer3202/pThr205 phosphorylation of tau, a post-translational modification implicated in the formation of tau inclusions in several tauopathies. We confirmed the degree of tau hyperphosphorylation proteostasis dysfunction by exposing neurons to OA and evaluating phosphorylated tau (pSer202/pThr205) via immunofluorescence (Figure 26A). Upon OA treatment, primary

cortical neurons displayed significantly higher phosphorylated tau (p-Tau) puncta as well as larger area (Figure 26B-C). Hence, as expected, OA-mediated phosphatase inhibition leads to the formation and accumulation of pathological tau inclusions in neurons.

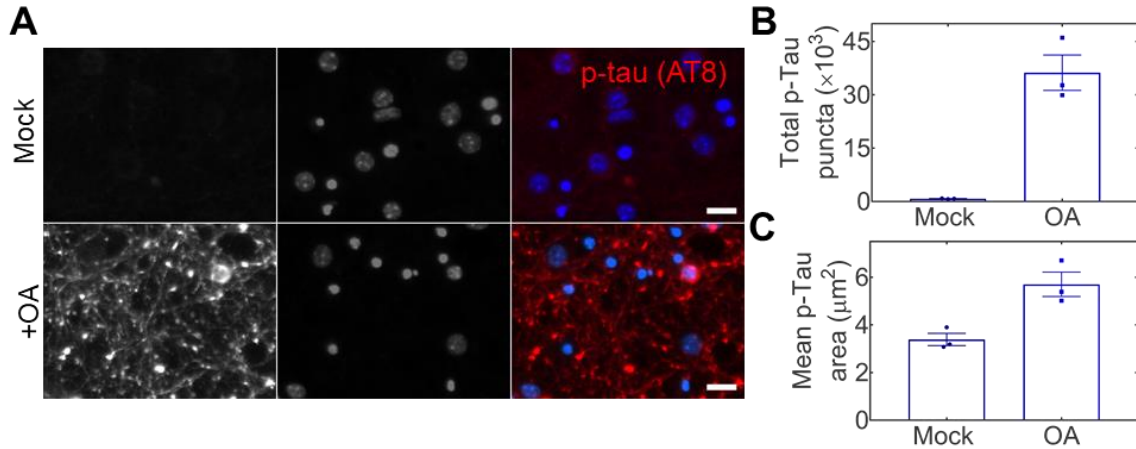


Figure 26: Formation of pathological tau following phosphatase inhibition in neurons. (A) Representative images showing phosphorylated tau (p-Tau) as detected by immunocytochemistry. (B) Image analysis revealed significantly higher total p-Tau puncta and (C) p-Tau area.

It has been reported that OA treatment in neuronal cultures can lead to increased activation levels of eIF2 α , an upstream modulator of ATF4 translation⁷⁵. The timescale of induction and overall temporal profile remains to be determined. Following confirmation of effective phosphatase inhibition in neurons, we used our stress-dependent expression vectors to examine whether we could detect the neuronal stress response associated with OA-mediated proteostasis impairment. Time-lapse microscopy images show the progression of ATF4 translational induction following OA treatment as reflected by ATF4GFP fluorescence (Figure 27A). At higher OA concentrations, the resulting kinetic curve demonstrates a sharp increase following an inflection point 4 h post-treatment while plateauing 20 h after induction. At lower concentrations, a similar kinetic pattern is maintained, albeit at a substantially smaller amplitude. We did not observe major

differences across groups in GFP expression when expressed constitutively (Figure 27B). Collectively, our results yield kinetic information into the neuronal stress response following phosphatase inhibition in neurons.

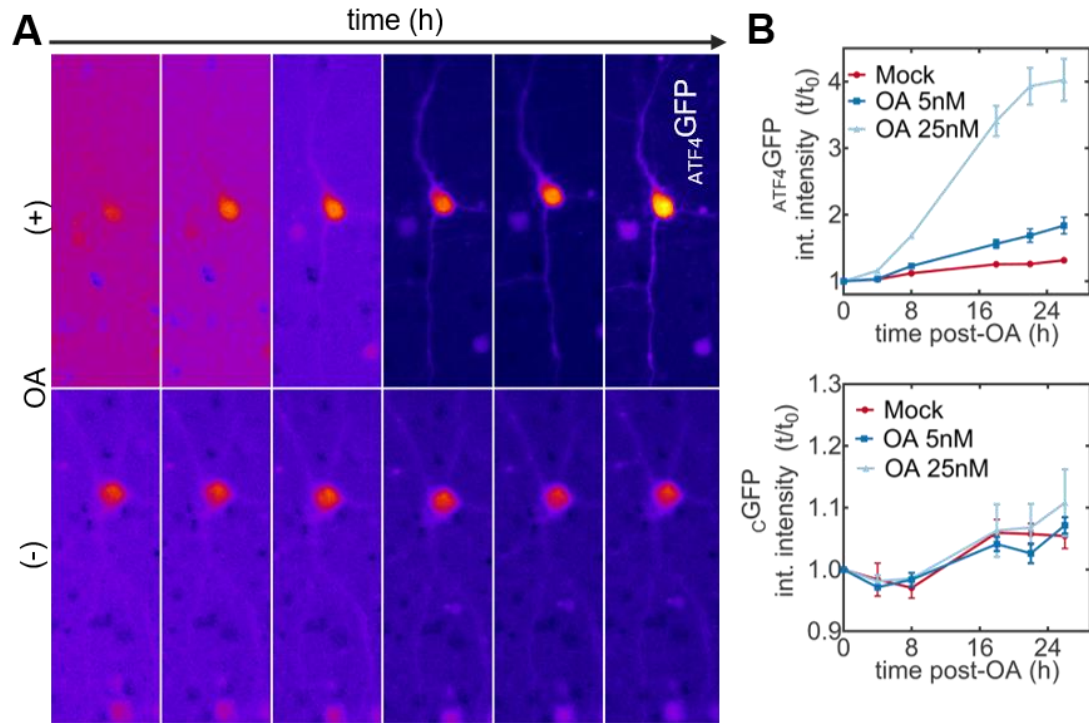


Figure 27: Kinetic profile of neuronal stress following phosphatase inhibition. (A) Representative images from timelapse studies examining $ATF4GFP$ levels in primary cortical neurons treated with okadaic acid (OA). (B) Corresponding kinetic curves for two different doses of OA in neurons expressing either $ATF4GFP$ (top) or $cGFP$ (bottom).

4.3.3 Mutant α -synuclein overexpression elicits a neuronal stress response

The A53T point mutation in α -syn (α -syn(A53T)) is implicated in familial forms of Parkinson's Disease (PD)¹¹⁷. Biochemical studies on α -syn(A53T) have shown the mutation confers an increased aggregation behavior compared to wild-type α -syn¹¹⁸. As a disease model, overexpression of α -syn(A53T) is known to lead to a neurodegenerative phenotype^{119,120}.

Overexpression of α -syn(A53T) overexpression in neurons impacts proteostasis by increasing the burden of protein synthesis, particularly the synthesis of an intrinsically disordered protein. To visualize neuronal stress responses to such proteostasis dysfunction, we overexpressed α -syn(A53T) and monitored $_{ATF4}GFP$ under different experimental conditions. We first asked whether α -syn(A53T) overexpression alone was sufficient to elicit detectable levels of $_{ATF4}GFP$ in neurons. We observed that at 10 d after lentiviral transduction, $_{ATF4}GFP$ levels were significantly higher in neurons overexpressing α -syn(A53T) than in α -syn(A53T)-negative controls (Mann Whitney test; $p=0.0002$; $n=8$; Figure 28). Thus, similar to prior work demonstrating UPR induction in the *SNCA* triplication model of PD⁵⁷, our results suggest UPR engagement in neurons overexpressing α -syn(A53T).

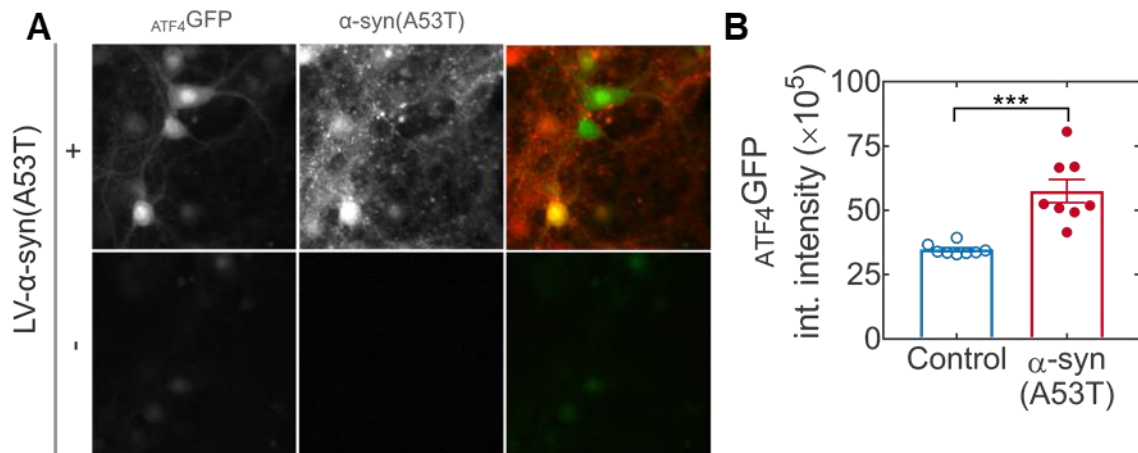


Figure 28: Induction of cellular stress in primary neurons at 10 d after the co-transduction with $_{ATF4}GFP$ and mKate2-tagged α -syn(A53T) vectors. (B) Quantification of $_{ATF4}GFP$ integrated intensity in neurons with (red) or without (blue) α -syn(A53T) expression. * $p = 0.0002$ by two-tail Mann-Whitney test.**

4.3.4 Mutant α -synuclein influences the neuronal response to ER stress

We then asked whether α -syn(A53T), an aggregation-prone, non-ER client protein, could influence neuronal susceptibility to ER stress. In addition to prominent protein misfolding, ER stress is considered a disease co-factor in many neurodegenerative conditions. Therefore, the temporal response of neurons subjected to such a level of combined proteostasis dysfunction remains a key question in understanding how α -syn(A53T) contributes to neurodegenerative outcomes. Following a 50-h time-lapse study, representative microscopy images show induction of UPR captured by $ATF4$ GFP expression in α -syn(A53T), TG, and TG with α -syn(A53T) treated neurons (Figure 29A-B). The corresponding kinetic curves of primary neurons expressing α -syn(A53T) and treated with TG showed a two-fold increase in $ATF4$ GFP over neurons treated with TG alone (Figure 29C). Notably, while $ATF4$ GFP induction in response to α -syn(A53T) is evident (Figure 29C, insert), it remained well below the more acute TG-induced stress.

To further assess the impact of α -syn(A53T) on TG-induced stress, we assayed for LDH release into the cell supernatant as an indicator of cellular health. We found that the presence of α -syn(A53T) sensitized neurons to LDH release following treatment with TG (Figure 30A). Altogether, we conclude that overexpression of α -syn(A53T) can predispose neurons to increased vulnerability in conditions of ER stress.

To further look into the interaction between α -syn(A53T) and ER stress, we hypothesized that ER stress could lead to increased intracellular aggregation of α -syn(A53T). In yeast, ER stress caused by reducing conditions (dithiothreitol) or glycosylation inhibition (tunicamycin) is sufficient to induce the aggregation of cytosolic, non-ER targeted proteins¹²¹. In the presence of tunicamycin, α -syn shows enhanced aggregation propensity in dopaminergic neurons⁶⁶. To evaluate this notion but with TG-

induced ER stress, we quantified the coverage area by α -syn(A53T) following TG-induced ER stress by tracking the mKate2 red fluorescence puncta. Contrary to other inducers of ER stress, our results show similar α -syn(A53T) area over time in the presence or absence of TG, which implies no enhanced visible α -syn(A53T) aggregation (Figure 30B).

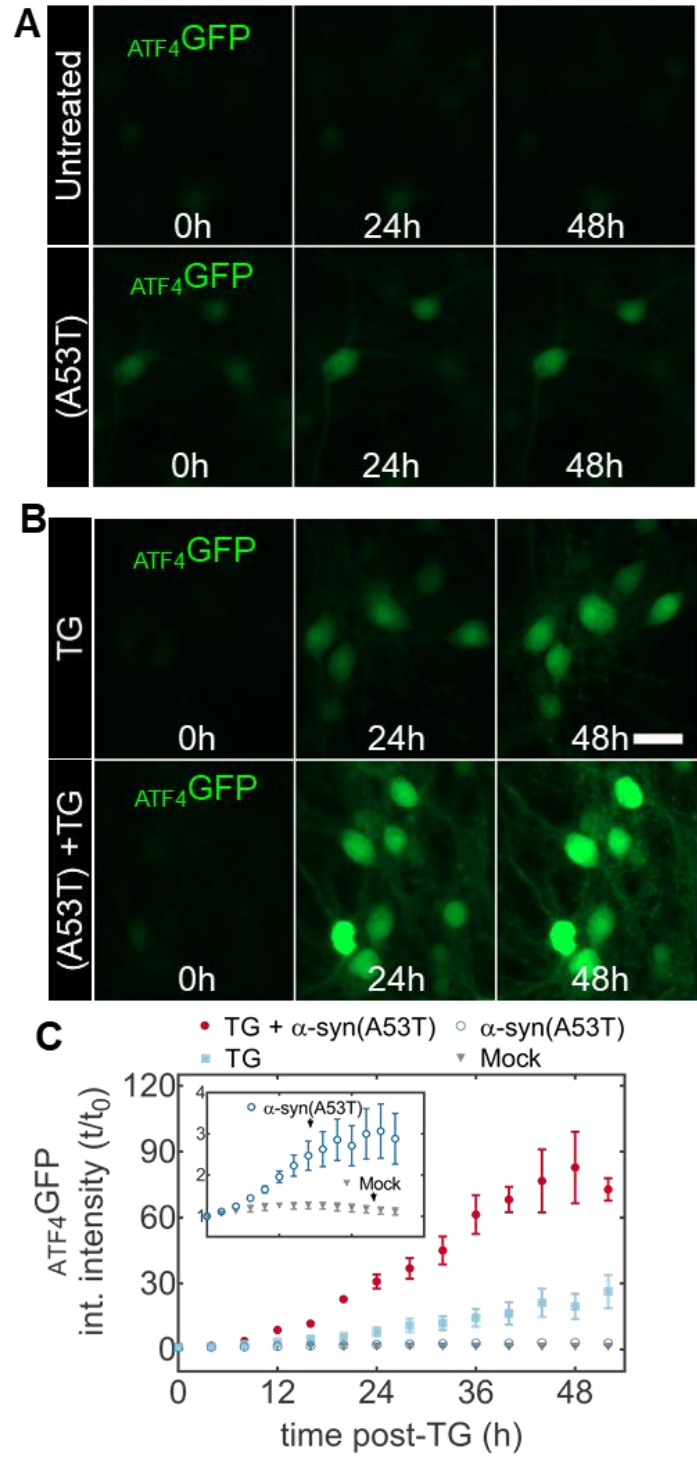


Figure 29: (A) Representative time-lapse microscopy images from neurons expressing ATF4GFP and left untreated (top) or subjected to α -syn(A53T) overexpression (bottom). (B) Neurons expressing ATF4GFP and exposed to TG stress (top) or a

combination of α -syn(A53T) and TG (bottom). Scale bar = 50 μ m. (C) Corresponding kinetic plots for the mean ATF4GFP integrated intensity for all groups.

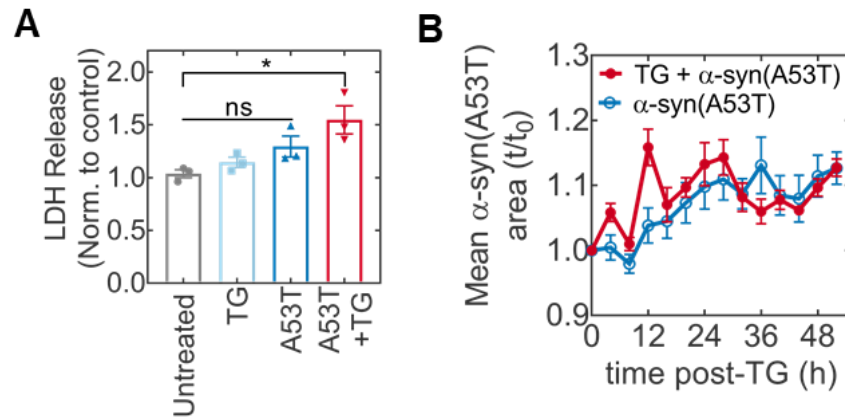


Figure 30: Cellular health and aggregation following α -syn overexpression in neurons. (A) Assessment of cellular health via LDH quantification in cell media. Absorbance values are normalized to an untreated control. Multiple comparisons by Kruskal-Wallis test (untreated vs A53T+TG $*p = 0.0395$; rest not significant. (B) Quantification of mean α -syn(A53T) area (red fluorescence positive puncta) with (closed circles) or without (open circles) TG stress.

CHAPTER 5. EFFICACY ASSESSMENT OF STRESS-DEPENDENT MANF EXPRESSION

5.1 Introduction

The mesencephalic astrocyte-derived neurotrophic factor (MANF) is a 20kDa protein first discovered as a glial-secreted neuroprotective agent specific to dopaminergic neurons^{122,123}. From structural analysis, it was identified that MANF contains a signal peptide for retention in the ER from where it can then be cleaved and secreted¹²⁴. It is important to note, however, that the physiological conditions that regulate MANF secretion and activity remain under investigation. The leading hypothesis postulates that MANF functions as an ER-resident protein to counteract ER stress by antagonizing BiP¹²⁵, an upstream modulator of the ER's unfolded protein response. Consistent with this notion, downregulation of endogenous MANF *in vivo* leads to sustained activation of the UPR, albeit without an apparent neurodegenerative phenotype in dopaminergic neurons. On the other hand, *in vitro*, MANF deficient neurons are more vulnerable to conditions of ER stress¹²⁶. Hence, MANF activity and secretion appears to have a role in ER stress.

MANF has gained attention primarily due to its neuroprotective properties leading to its application in several neurodegenerative contexts (Table 3). When expressed in primary neuronal cultures, MANF exhibits enhanced neuroprotective activity when compared to the classical glial-derived or brain-derived neurotrophic factors¹²³. When delivered as a recombinant protein or via an expression vector, MANF protects neural cells from insults such as 6-hydroxydopamine (6OHDA)¹²⁷, amyloid- β ¹²⁸, and staurosporine¹²⁹.

For applications *in vivo*, MANF gene delivery has shown promise in rodent models of stroke and parkinsonian mimetic toxins.

Table 3: Literature review summarizing the neuroprotective efficacy of MANF

<i>System / Model</i>	Insult / Deficit	MANF format	Treatment details	Assessment	Reference
<i>In vivo (Rat)</i>	STR 6-OHDA	AAV9-hMANF	Intrastriatal injection 10 days post 6-OHDA	Amphetamine rotations TH assessment in STR and SNpc	127
<i>In vitro (SH-SY5Y)</i>	6-OHDA	Recombinant human MANF	rMANF co-incubated with 6-OHDA	MTT assay	127
<i>In vitro (SH-SY5Y)</i>	6-OHDA	pAAV-hMANF	Analyzed 24 or 48 h post-transfection	MTT assay UPR WB	127
<i>In vitro (N2a)</i>	A β ₍₁₋₄₂₎	MANF-flag plasmid	Analyzed 24 h post-transfection	MTT assay UPR WB	128
<i>In vitro (SH-SY5Y)</i>	A β ₍₁₋₄₂₎	Recombinant human MANF	rMANF pre-treatment 4 h before insult	MTT assay UPR WB	128
<i>In vivo (Rat)</i>	Cortical stroke	Recombinant MANF	Intracerebral infusion	DCX+ cell migration	130
<i>In vivo (Rat)</i>	MCAo-stroke	AAV7-MANF and rMANF	Treatment 1 d post lesion	Lesion volume Behavior Immunophenotype	131
<i>In vitro (SCG)</i>	Staurosporine NGF withdrawal	MANF plasmid	Microinjection at DIV5	Viability assay 3 d post-insult	129
<i>In vivo (rat)</i>	STR 6-OHDA	Recombinant human MANF	MANF STR injections 6 h before or 4 wk after 6-OHDA lesion	Behavior TH assessment	132
<i>In vivo (rat)</i>	STR 6-OHDA	LV-MANF	Intranigral or intrastriatal injections at time of lesion	TH assessment Behavior	133
<i>C. elegans</i>	MANF mutants	Vs MANF wildtype	-	Degeneration Alpha-synuclein aggregation	134

5.2 Methods

Cell culture

Mouse neuroblastoma Neuro-2a (N2a) cells (a gift from Dr. Gary Bassell) were maintained in a humidified 5% CO₂ atmosphere at 37 °C in complete medium consisting of Dulbecco's Modified Eagle's medium (DMEM) supplemented with 10% fetal bovine serum, 2 mM L-glutamine, 100 international units (IU)/mL penicillin, and 100 µg/mL streptomycin. Cells were used in their undifferentiated state for studies described herein.

Plasmid construction and vector production

To generate stress-dependent expression vectors encoding MANF, we modified our original _{ATF4}GFP vectors by cloning MANF-FLAG from a pcDNA3.1 vector downstream of GFP linked by a P2A self-cleaving sequence. A similar construct lacking the ATF4 cassette was produced as a control for the constitutive expression of MANF-GFP. Transgene expression in both constructs is driven by the chicken β-actin (CBA) promoter for ubiquitous expression in mammalian cells. The correct sequences were confirmed by digestion analyses and DNA sequencing. MANF vectors are summarized in Figure 31.

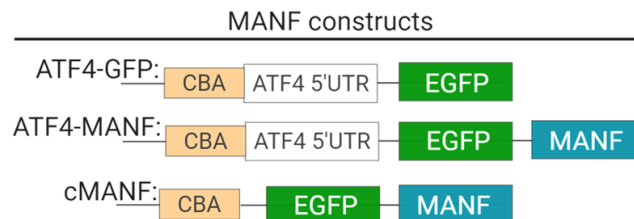


Figure 31: Constructs for the expression of the mesencephalic astrocyte-derived neurotrophic factor (MANF) either constitutively or ATF4-controlled.

Expression characteristics of each plasmid were evaluated in N2a cells by transient transfection using LipofectamineTM 3000 (Thermo Fisher Scientific).

Pharmacological treatments

Thapsigargin (Sigma) was solubilized in DMSO and working solutions were prepared in DMEM maintenance medium. From working solutions, drugs were added directly to the cells at the appropriate final concentration. 6-hydroxydopamine (6OHDA) was solubilized in DPBS containing 0.02% ascorbic acid to prevent auto-oxidation. Solvent-only solutions were used as the control for each drug, accordingly. Culture medium was not replaced after treatment to avoid additional disturbances.

Image acquisition and analysis

Live-cell imaging experiments were conducted using a Cytation 5 Cell Imaging Multi-Mode Reader (Biotek Inc.) equipped with a gas controller for CO₂ control and 4-zone temperature incubation with condensation control. Fluorescent images were acquired with a 10X phase contrast objective using the GFP built-in LED filter cubes. The image acquisition routine was established in the Gen5 Plus software to follow a kinetic read taking at least 12 images in the same x- and y-coordinates for each well throughout the course of each time-lapse session.

Raw images were subjected to semi-automated pixel-based analysis using the Gen5 image analysis function. For reporter analysis and cell counts, threshold settings were adjusted to capture GFP positive cells. Image analysis metrics (GFP counts and GFP intensity) were calculated for each image in an experiment using the same threshold and masking settings.

Calculated metrics were normalized to the correspondent first reading (t_0) to express a relative rate of change from baseline.

Statistics

Statistical analysis was performed in Graph Pad Prism 7. Data sets were tested for normality using the D'Agostino and Pearson test. Multiple group comparisons were analyzed by one-way ANOVA followed by a Tukey post-hoc. Results are reported as mean \pm SEM.

5.3 Results

5.3.1 Characterization of ATF4-MANF constructs

The objective of this study was to evaluate the feasibility of MANF delivery via stress-controlled expression vectors. To this purpose, we modified our ATF4-controlled expression vectors to incorporate a transgene insert encoding for MANF resulting in $_{ATF4}$ MANF-GFP. For proper efficacy assessment, we generated vectors for the constitutive expression of MANF ($_c$ MANF) as they have been demonstrated to be neuroprotective in previous studies.

Using N2A neuroblastoma cells, we first verified that the stress-dependent expression conferred by the 5'UTR ATF4 sequence remained intact following the incorporation of the MANF sequence. Transiently transfected N2A cells with $_c$ MANF, $_{ATF4}$ MANF-GFP, or $_{ATF4}$ GFP were exposed to a 24 h treatment with the ER stressor thapsigargin (TG). Image analysis of the GFP fluorescent output revealed a stress-

dependent increase in fluorescent levels based on TG treatment. These expression characteristics were not observed in the case of cMANF given its constitutive nature.

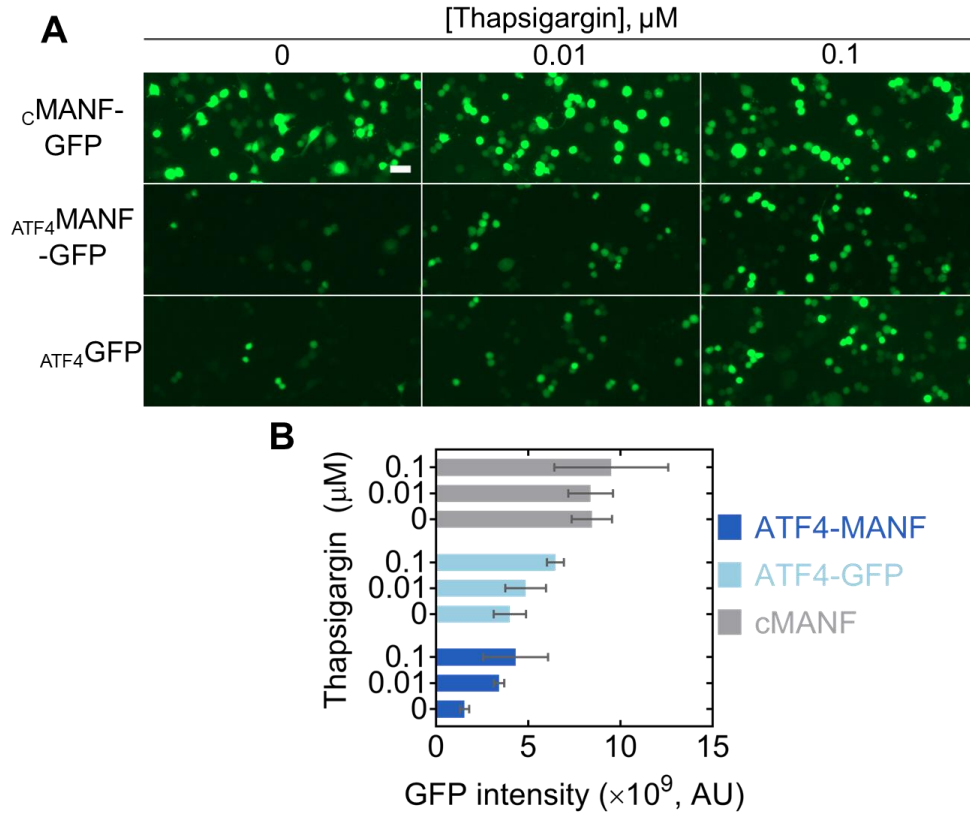


Figure 32: Stress-dependent expression of MANF in N2a cells following treatment with thapsigargin (TG) for 24 h. (A) Representative microscopy images and (B) corresponding quantification of GFP intensity.

5.3.2 MANF cytoprotection in an *in vitro* model of cellular stress

To evaluate cytoprotection, we opted for the 6OHDA model of cellular stress given the performance of MANF in counteracting 6OHDA-induced toxicity reported in previous studies. The addition of 6-OHDA took place 24 h after transfection once transgene expression was confirmed by fluorescence microscopy. At the two 6OHDA doses tested, cell loss reached over 50% or more at ~6 h post-treatment (Figure 33A). Among the treatment groups, only cells expressing cMANF showed a modest reduction in toxicity

when compared to the rest of the 6OHDA-treated groups (Figure 33B). Moreover, in the absence of 6OHDA, cMANF appeared to improve cellular proliferation as reflected in a higher number of identified GFP⁺ cells. In contrast, ATF4-MANF-GFP did not result in any apparent improvement in cell viability following exposure to 6OHDA. These results collectively lead us to conclude that stress-responsive MANF delivery would not likely be a useful strategy in astringent neurodegenerative models such as those induced by 6OHDA.

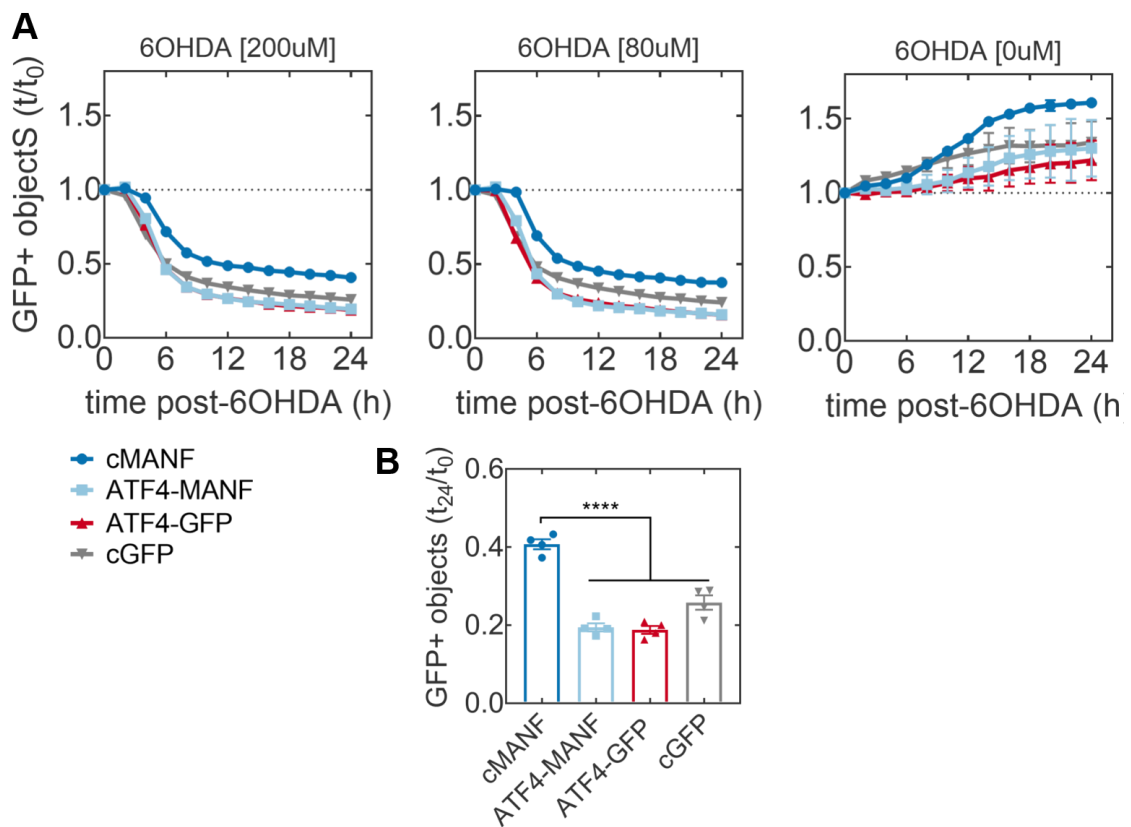


Figure 33: Timelapse monitoring of cell counts following exposure to the neurotoxin 6-hydroxydopamine (6OHDA). N2a cells were transfected with either cMANF, ATF4-MANF, ATF4-GFP, or cGFP and exposed to 200 or 80 μ M 6OHDA. Multiple group comparisons were analyzed by one-way ANOVA followed by a Tukey post-hoc ($p < 0.0001$, $n = 4$ biological replicates).

CHAPTER 6. DISCUSSION AND RECOMMENDATIONS FOR FUTURE WORK

This dissertation describes the development and characterization of stress-dependent expression vectors to monitor proteostasis dysfunction in neurons. We first show how AAV-based reporter constructs can harness the selective translation of ATF4 mRNA as part of the induction of the UPR to yield a quantifiable readout suitable for non-cell destructive kinetic monitoring of cellular stress due to calcium dysregulation in the ER. We extend our characterization studies to non-ER targeted perturbations and present data that describes the temporal profile of stress progression and cell loss in neurons experiencing global inactivation of the proteasome machinery. Finally, we adopt the overexpression of α -syn(A53T) in neurons, an established *in vitro* model of PD, and describe the impact of α -syn(A53T) eliciting cellular stress and influencing neuronal susceptibility to ER stress.

6.1.1 *Insights into neuronal proteostasis*

Proteostasis dysfunction is an important manifestation in all major neurodegenerative diseases. However, while analysis of proteostasis dysfunction via fluorescent reporters of UPR activation has been previously reported⁸², these molecular tools have not been incorporated into neurobiologically relevant contexts. Herein, we report our initial efforts towards adapting such technologies for use in neurobiological research. Using mouse primary neurons as a cellular system, our results demonstrate the induction characteristics of ATF4GFP expression as a surrogate for ER stress and UPR activation in a cell-based assay

suitable for high-throughput screening studies. Cell-based assays amenable for non-destructive longitudinal monitoring, and with the dynamic range to either capture acute (e.g. thapsigargin) or chronic (e.g. α -synuclein) stress responses, could have an impact on neuroscience discovery research and beyond. For example, such assays could facilitate a more refined understanding of the mechanisms of action as well as time-cellular fate relationships in the search for pharmacological modulators of the UPR. Besides neurodegeneration, UPR activation, particularly PERK signaling, is central to the development of human diseases like pancreatic β -cell dysfunction in diabetes, inflammation, atherosclerosis, and diabetes¹³⁵. Therefore, a wide range of applications exists for which a cell-based assay for stress detection compatible with primary cell sources and kinetic monitoring would be of great benefit.

The ubiquitin-proteasome system is one of the two identified protein degradation pathways in eukaryotic cells contributing to the efficient degradation and turnover of proteins. Pharmacological blockade of the proteasome is an established perturbation to proteostasis leading to cellular stress and eventually cell death. In HeLa cells, proteasome inhibition with MG132 results in stress granules in a response coordinated by the GCN2-eIF2 α axis of the ISR¹³⁶. In contrast, prior work in neural-like cells and rat neurons identified the activation of PERK as an event in the cellular response to different types of proteasome inhibitors⁷⁹. In addition to supporting the notion of UPR engagement, our work provides kinetic data to describe the progression of neuronal stress following proteasome inhibition in neurons.

Furthermore, consistent with previous findings in non-neuronal systems, our results indicate a clear relationship between the temporal progression of stress induction and cell

death. Notably, visualizing asynchronous cell death within a cell population, a process in which only 5-10% of cells will execute apoptosis at any given moment, represents a technical challenge¹⁰³. By examining neuronal stress using live-cell imaging, we distinguished neuronal death asynchronism and correlate the time of cell loss with maximum stress levels. The relationship between stress progression and induction of a specific mechanism of cell death remains to be explored. Consistent with our measurement of an ATF4-based reporter signal, the most likely cell death mechanism following sustained UPR activation is mediated by CHOP, an ATF4-target gene that orchestrates apoptosis²⁶. However, given the acute nature of MG132 treatment, we cannot discard the contribution of other factors such as oxidative stress in the cytotoxicity that we observe.

6.1.2 Insights into the influence of α -synuclein on ER stress

The presence and accumulation of misfolded species of α -synuclein are recognized as important contributors to neurodegeneration in Parkinson's Disease (PD) as well as neurodegenerative conditions collectively known as α -synucleinopathies. In addition to PD, major α -synucleinopathies include Dementia with Lewy Bodies (DLB) and Multiple Systems Atrophy (MSA). In each condition, it is believed that α -syn pathogenicity stems from conformational changes that lead to fibrillar cellular inclusions referred to as Lewy pathology, of which α -syn is the main component^{51,137}. When in excess, such as a result of duplication or triplication of the SNCA gene, wild-type α -syn can trigger early-onset PD^{110,111}. Additionally, human genetics has identified six mutations in the gene encoding α -syn (SNCA) to be linked to familial forms PD. In particular, the A53T α -syn point mutation is linked to early-onset PD in humans¹¹⁷. Mutant α -syn(A53T) displays faster fibrilization and aggregation behavior at a molecular level compared to wild-type α -syn¹¹⁸.

We overexpressed mutant α -syn(A53T) in wild-type background of primary neurons to determine whether our $_{ATF4}GFP$ reporter assay could capture stress responses arising from such manipulation to neuronal proteostasis. While the overexpression model of α -syn(A53T) does not yield insoluble inclusions *in vitro*, multiple lines of evidence suggest that α -syn oligomers can elicit toxicity without the need of forming high molecular weight aggregates^{138,139}. Our studies found that the overexpression of α -syn(A53T) alone could produce detectable levels of stress 10-d post-transduction of α -syn(A53T). How this level of stress response relates with known manifestations of α -syn(A53T) such as mitochondrial dysfunction¹⁴⁰ or axonal degeneration¹³⁸ warrants further investigation. In future studies, our lab plans to explore these research questions in improved disease-relevant systems using human induced pluripotent stem cell-derived dopaminergic neurons harboring a site-specific mutation for A53T.

The study of the interaction between α -syn and other disease co-factors is an active area of research. Given the intricacies of the pathophysiology of conditions such as PD, the most likely description of disease pathophysiology includes the combination of aggregation-prone proteins such as α -syn and co-factors, including aging, ER stress, and neuroinflammation. It has been hypothesized that proteinaceous inclusions in neurodegenerative diseases could be a consequence of an overall decline in proteostasis due to aging¹⁴¹. Proteostasis function can also be affected by other factors such as neuroinflammation via increased ER stress¹⁴². We examined whether the presence of α -syn(A53T) influenced the degree of the neuronal response to ER stress. Whether the presence of α -syn(A53T) lowers the threshold or simply amplifies UPR signaling remains to be fully elucidated. However, our data indicate that, with α -syn(A53T) overexpression,

neurons elicit a more robust stress response to ER stress induced by thapsigargin. Furthermore, our results suggest a degree of increased vulnerability where cellular health is compromised due to the combined effect of α -syn(A53T) and thapsigargin-induced ER stress in neurons. This observation is consistent with previous studies indicating that, in the context of PD, a secondary insult (e.g., environmental factor) is needed to induce cell death⁹⁸.

6.1.3 Opportunities for added functionality as a reporter construct

Future iterations of the approach presented herein should focus on certain opportunities for extended functionality. Detection of neuronal stress responses using an ATF4-based reporter only captures the timescale of UPR activation as directed by PERK signaling. However, the IRE1 arm of the UPR has also been recognized as a critical pathway mediating the UPR in neurodegeneration. A future design where BiP controls the stress-dependent expression vector, as an upstream modulator of both IRE1 and PERK, could capture a global stress response and bypass any variability in IRE1 and PERK signaling.

The focus of the work presented in this thesis is on the unfolded protein response of the ER. However, recently, organelle-specific UPR signaling such as mitochondrial UPR has gained more attention (reviewed by Shpilka and Haynes, 2018¹⁴³). To study the temporal induction of organelle-specific UPR, this ATF4-based reporter could be modified with organelle-specific targeting sequences, which will allow the signal to be restricted to a particular organelle such as the mitochondria. Similarly, previous work has described compartment-specific (cell body vs. processes) stress responses directed by the local translation of ATF4 in axons¹⁴⁴. A construct design that would incorporate cell

compartment-specific localization signals would allow for such subcellular analyses. Additionally, by incorporating cell-type specific promoters, stress-responsive AAV constructs could enable a direct assessment of how different neuronal subtypes respond to proteostasis impairment, further illuminating specific neuronal vulnerabilities in disease. Finally, translating this approach *in vivo* could enable stress-dependent labeling of distinct neuronal populations in the CNS following chemical or genetic-based stressors.

6.1.4 *Opportunities for use as a stress-responsive gene therapy*

We envisioned a stress-responsive gene therapy approach that could deliver a corrective measure to prevent cell death upon induction of stress by a neurodegenerative insult. This therapeutic paradigm, termed physiologically-responsive gene therapy¹⁴⁵, could potentially avoid unnecessary toxicity and side effects associated with the overstimulation of a biological target.

Following the characterization of stress-dependent expression vectors, we opted to incorporate MANF; a neurotrophic factor believed to hold great promise as a neuroprotective therapy. To date, it has not yet been elucidated whether MANF can effectively prevent cell death associated with proteostasis dysfunction. However, initial neuroprotective studies have shown that MANF can protect neurons from neurotoxins such as 6OHDA. For this reason, we tested our stress-dependent MANF vectors in an *in vitro* model of 6OHDA. Our data suggest that the cell damage due to such neurotoxic insult occurs at a much shorter timescale than that needed for the stress-induced expression and corrective action of MANF. As observed with the constitutive expression of MANF, when the protein is already being expressed, neural cells can counteract 6OHDA toxicity.

However, it is important to note that previous work has reported on the efficacy of recombinant MANF when co-added to neural cells together with 6OHDA¹²⁷. Therefore, we believe that the absence of neuroprotective activity we observed with ATF4-controlled MANF expression is because of the lack of proper induction for sufficient protein expression in a timely manner to exert its biological activity.

Future work can primarily address these limitations by systematically evaluating the efficacy of MANF in chronic models of neurodegeneration. For example, inducible genetic models of α -synuclein expression would provide pharmacological control of α -syn burden to adjust for severity¹⁴⁶. Alternatively, the use of preformed fibrils of α -syn (PFF- α -syn) could elicit a dose-dependent level of α -syn pathology within a 7-10 d period¹⁴⁷. However, the degree to which the PFF- α -syn model engages the UPR remains unclear. Importantly, like other neurotrophic factors, MANF displays enhanced neuroprotection to selective neuronal subtypes. In particular, MANF appears to protect dopaminergic neurons selectively¹²³. For this reason, for efficacy studies, the biological activity of MANF would be better assessed in primary or stem cell-derived dopaminergic cultures.

The stress-dependent expression vectors presented in this work could also serve as a platform system into which different therapies could be plugged in. We, therefore, envision opportunities for future work where an unbiased approach, where multiple biologics are screened, could yield candidates with neurorestorative potential.

6.1.5 Opportunities for a cell non-autonomous therapeutic approach

As part of our initial characterization of ATF4-controlled expression vectors, we observed a robust response to conventional ER stress inducers by astroglia. While

characterizing whether this response represented a proinflammatory phenotype was beyond this project's scope, previous reports have identified neuroinflammation as a contributor to ER stress¹⁴². Therefore, it remains plausible that a neuroinflammatory milieu could induce ATF4-dependent stress in glial cells.

The generation of stress-responsive vectors for gene therapy responds to the need to avoid unregulated transgene expression in neurons. A physiologically-responsive gene therapy leverages physiological changes in the host to control transgene expression¹⁴⁵. While this project targeted neurons, future work could harness physiological changes in non-neuronal cells (e.g., astrocytes) to achieve the desired outcome but in a cell non-autonomous manner. For instance, given our observations in glia, an alternative approach could be to mobilize these brain-resident cells to generate a therapeutic product *in situ*. In fact, we have previously demonstrated the engineering of viral vectors capable of expressing a cell-permeable protein product that is secreted out of the virally-infected neurons to affect neighboring cells^{113,148}.

CONCLUSIONS

In conclusion, this work presents the development and characterization of stress-dependent expression vectors that enable the longitudinal study of neuronal responses to ER stress and proteostasis dysfunction in live neurons. Thus, these results demonstrate the feasibility of mobilizing cellular stress signaling to create physiologically-responsive viral vectors for use in neuroscience. Additionally, by using these constructs in a reporter assay, we learned that during unresolved stress, neuronal death is preceded by a relative maximum induction of the UPR. Furthermore, our work enabled the study of how the Parkinson's-related mutant protein α -syn(A53T) influences the neuronal stress response.

As key contributions, this work bridges the gap between advances in the live-cell analysis of cellular responses to proteostasis dysfunction and their application in neurobiology. By adopting an experimental approach like the one presented herein, neurobiologists can now shed light on mechanisms of neurodegeneration associated with the induction of neuronal stress responses. Collectively, we hope this work will stimulate the study of the temporal activation of the UPR in neurons. Finally, this work establishes the foundation for a stress-induced gene therapy approach. While our *in vitro* results do not support the use of MANF for this purpose, our approach could be easily modified to provide therapeutic benefit in other contexts.

APPENDIX A. METHOD SUMMARY FOR NEURITE ANALYSIS USING CELLPROFILER

We used the open-source image analysis software CellProfiler¹⁴⁹ to conduct phenotypic characterization of immunostained cell samples. A custom-made algorithm uses a morphological marker (e.g., TUJ1) to threshold neurons in each field. The next step is to identify soma (cell bodies) as primary objects based on size. Neurites are then identified as secondary objects (nested within the primary objects step) and subjected to a smoothing filter. The resulting image is then ‘skeletonized’ using the MorphNeurites processing step. As an output, this process generates data sets for neurite length, branches, and end points (terminals).

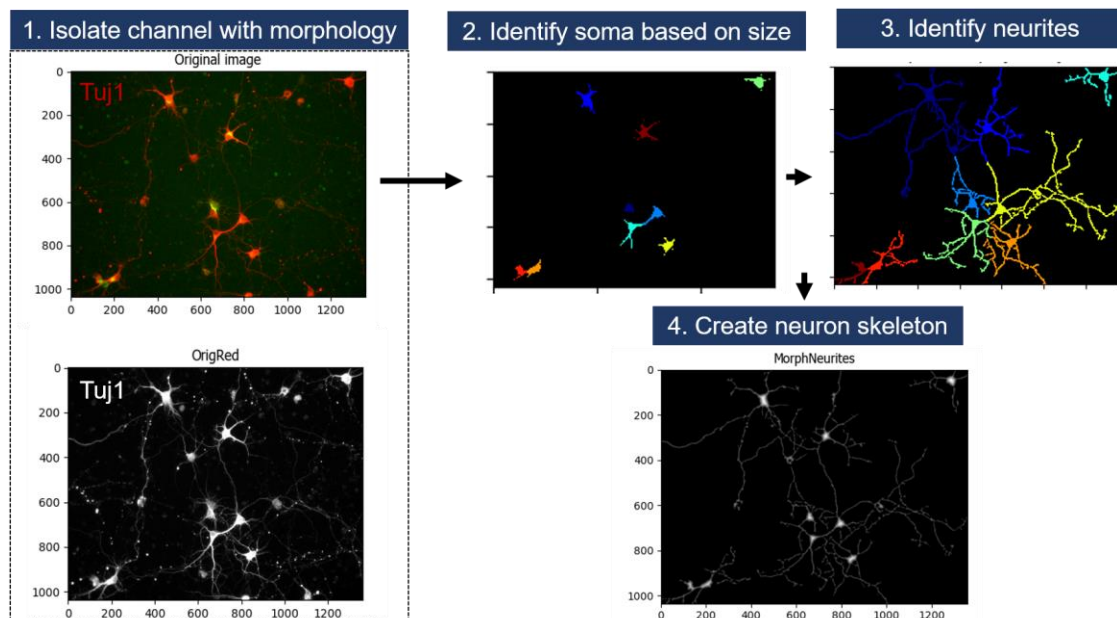


Figure 34: Algorithm for neurite analysis using CellProfiler

APPENDIX B. PHD WORK SUMMARY (2014-2020)

Titles of scientific work published or presented during my PhD but not described in this dissertation:

Santiago-Lopez, A.J., et al. In Vivo Assessment of Cell Death and Nigrostriatal Pathway Integrity following Continuous Expression of C3 Transferase. *Neuroscience* 442, 183-192 (2020)

Santiago-Lopez, A.J., et al. C3 Transferase Gene Therapy for Continuous RhoA Inhibition. *Methods in Molecular Biology*, 267-281 (2018)

Sei, Y. J.; Ahn, J.; Kim, T.; Shin, E., **Santiago-Lopez, A. J.**, Jang, S. S.; Jeon, N. L.; Jang, Y. C.; Kim, Y. Detecting the functional complexities between high-density lipoprotein mimetics. *Biomaterials* 170, 58–69 (2018)

Probing Biomolecular Interactions of HDL mimetics Nanomaterials and the Amyloid-beta Peptide for the Treatment of Alzheimer’s Disease. **Biomedical Engineering Society Conference**. Minneapolis, MN. (2016)

Microfluidic Reconstitution of HDL-apoE for CNS Therapeutics. **Biomedical Engineering Society Conference**. Tampa, FL. (2015)

REFERENCES

1. Gooch, C. L., Pracht, E. & Borenstein, A. R. The burden of neurological disease in the United States: A summary report and call to action. *Ann Neurol* **81**, 479–484 (2017).
2. Yang, G. *et al.* Economic Burden and Future Impact of Parkinson’s Disease - Final Report. *Michael J. Fox Found. - Lewin Group, Inc.* **July**, 1–64 (2019).
3. Kowal, S. L., Dall, T. M., Chakrabarti, R., Storm, M. V. & Jain, A. The current and projected economic burden of Parkinson’s disease in the United States. *Mov. Disord.* **28**, 311–318 (2013).
4. Ciechanover, A. & Kwon, Y. T. Degradation of misfolded proteins in neurodegenerative diseases: therapeutic targets and strategies. *Exp. Mol. Med.* **47**, e147–e147 (2015).
5. PhARMA. *Medicines in Development for Neurological Disorders.* (2018).
6. Wang, D., Tai, P. W. L. & Gao, G. Adeno-associated virus vector as a platform for gene therapy delivery. *Nat. Rev. Drug Discov.* **18**, 358–378 (2019).
7. Kotterman, M. A. & Schaffer, D. V. Engineering adeno-associated viruses for clinical gene therapy. *Nat. Rev. Genet.* **15**, 445–51 (2014).
8. Wright, J. F. Manufacturing and characterizing AAV-based vectors for use in clinical studies. *Gene Ther.* **15**, 840–848 (2008).

9. Shevtsova, Z., Malik, J. M. I., Michel, U., Bähr, M. & Kügler, S. Promoters and serotypes: targeting of adeno-associated virus vectors for gene transfer in the rat central nervous system *in vitro* and *in vivo*. *Exp. Physiol.* **90**, 53–59 (2005).
10. Manfredsson, F. P., Bloom, D. C. & Mandel, R. J. Regulated protein expression for *in vivo* gene therapy for neurological disorders: Progress, strategies, and issues. *Neurobiol. Dis.* **48**, 212–221 (2012).
11. Colella, P., Ronzitti, G. & Mingozi, F. Emerging Issues in AAV-Mediated *In Vivo* Gene Therapy. *Mol. Ther. - Methods Clin. Dev.* **8**, 87–104 (2018).
12. Kaemmerer, W. F. How will the Field of Gene Therapy Survive its Success? 166–177 (2018). doi:10.1002/btm2.10090
13. Ulusoy, A., Sahin, G., Björklund, T., Aebischer, P. & Kirik, D. Dose optimization for long-term rAAV-mediated RNA interference in the nigrostriatal projection neurons. *Mol. Ther.* **17**, 1574–1584 (2009).
14. Thomsen, G. M. *et al.* Systemic injection of AAV9-GDNF provides modest functional improvements in the SOD1 G93A ALS rat but has adverse side effects. *Gene Ther.* **24**, 245–252 (2017).
15. Manfredsson, F. P. *et al.* Nigrostriatal rAAV-mediated GDNF overexpression induces robust weight loss in a rat model of age-related obesity. *Mol. Ther.* **17**, 980–991 (2009).
16. Hipp, M. S., Kasturi, P. & Hartl, F. U. The proteostasis network and its decline in

ageing. *Nat. Rev. Mol. Cell Biol.* doi:10.1038/s41580-019-0101-y

17. Balch, W. E., Morimoto, R. I., Dillin, A. & Kelly, J. W. Adapting Proteostasis for Disease Intervention. *Science (80-.)*. **319**, 916–919 (2008).
18. Frakes, A. E. & Dillin, A. The UPRER: Sensor and Coordinator of Organismal Homeostasis. *Mol. Cell* **66**, 761–771 (2017).
19. Hetz, C. & Saxena, S. ER stress and the unfolded protein response in neurodegeneration. *Nat. Rev. Neurol.* **13**, 477–491 (2017).
20. Pakos-Zebrucka, K. *et al.* The integrated stress response. *EMBO Rep.* **17**, 1374–1395 (2016).
21. van Anken, E. *et al.* Specificity in endoplasmic reticulum-stress signaling in yeast entails a step-wise engagement of HAC1 mRNA to clusters of the stress sensor Ire1. *Elife* **3**, (2014).
22. Yoshida, H. *et al.* A time-dependent phase shift in the mammalian unfolded protein response. *Dev. Cell* **4**, 265–271 (2003).
23. Fink, E. E. *et al.* XBP1-KLF9 Axis Acts as a Molecular Rheostat to Control the Transition from Adaptive to Cytotoxic Unfolded Protein Response. *Cell Rep.* **25**, 212-223.e4 (2018).
24. Lin, J. H. *et al.* IRE1 Signaling Affects Cell Fate During the Unfolded Protein Response. *Science (80-.)*. **318**, 944–949 (2007).
25. Lin, J. H., Li, H., Zhang, Y., Ron, D. & Walter, P. Divergent effects of PERK and

- IRE1 signaling on cell viability. *PLoS One* **4**, 1–6 (2009).
26. Galehdar, Z. *et al.* Neuronal Apoptosis Induced by Endoplasmic Reticulum Stress Is Regulated by ATF4-CHOP-Mediated Induction of the Bcl-2 Homology 3-Only Member PUMA. *J. Neurosci.* **30**, 16938–16948 (2010).
 27. Li, S., Yang, L., Selzer, M. E. & Hu, Y. Neuronal endoplasmic reticulum stress in axon injury and neurodegeneration. *Ann. Neurol.* **74**, 768–777 (2013).
 28. Wouters, B. G. & Koritzinsky, M. Hypoxia signalling through mTOR and the unfolded protein response in cancer. *Nat. Rev. Cancer* **8**, 851–864 (2008).
 29. Grootjans, J., Kaser, A., Kaufman, R. J. & Blumberg, R. S. The unfolded protein response in immunity and inflammation. *Nat. Rev. Immunol.* **16**, 469–484 (2016).
 30. Naidoo, N., Ferber, M., Master, M., Zhu, Y. & Pack, A. I. Aging Impairs the Unfolded Protein Response to Sleep Deprivation and Leads to Proapoptotic Signaling. *J. Neurosci.* **28**, 6539–6548 (2008).
 31. Hussain, S. G. & Ramaiah, K. V. A. Reduced eIF2 α phosphorylation and increased proapoptotic proteins in aging. *Biochem. Biophys. Res. Commun.* **355**, 365–370 (2007).
 32. Nuss, J. E., Choksi, K. B., DeFord, J. H. & Papaconstantinou, J. Decreased enzyme activities of chaperones PDI and BiP in aged mouse livers. *Biochem. Biophys. Res. Commun.* **365**, 355–361 (2008).
 33. Paz Gavilán, M. *et al.* Cellular environment facilitates protein accumulation in aged

- rat hippocampus. *Neurobiol. Aging* **27**, 973–982 (2006).
34. Ron, P. W. and D. The unfolded protein response. *Science* (80-.). **334**, 1081–1086 (2011).
 35. Harding, H. P., Zhang, Y., Bertolotti, A., Zeng, H. & Ron, D. PERK is essential for translational regulation and cell survival during the unfolded protein response. *Mol. Cell* **5**, 897–904 (2000).
 36. Harding, H. P. *et al.* Regulated translation initiation controls stress-induced gene expression in mammalian cells. *Mol. Cell* **6**, 1099–1108 (2000).
 37. Carrara, M., Prisci, F., Nowak, P. R., Kopp, M. C. & Ali, M. M. U. Noncanonical binding of BiP ATPase domain to Ire1 and Perk is dissociated by unfolded protein CH1 to initiate ER stress signaling. *Elife* **2015**, 1–16 (2015).
 38. Bertolotti, A., Zhang, Y., Hendershot, L. M., Harding, H. P. & Ron, D. Dynamic interaction of BiP and ER stress transducers in the unfolded- protein response. *Nat Cell Biol* **2**, 326–32. (2000).
 39. Donnelly, N., Gorman, A. M., Gupta, S. & Samali, A. The eIF2 α kinases: Their structures and functions. *Cell. Mol. Life Sci.* **70**, 3493–3511 (2013).
 40. Hai, T. & Hartman, M. G. The molecular biology and nomenclature of the activating transcription factor/cAMP responsive element binding family of transcription factors: Activating transcription factor proteins and homeostasis. *Gene* **273**, 1–11 (2001).

41. Dey, S. *et al.* Both transcriptional regulation and translational control of ATF4 are central to the integrated stress response. *J. Biol. Chem.* **285**, 33165–33174 (2010).
42. Ameri, K. & Harris, A. L. Activating transcription factor 4. *Int. J. Biochem. Cell Biol.* **40**, 14–21 (2008).
43. Vattam, K. M. & Wek, R. C. Reinitiation involving upstream ORFs regulates ATF4 mRNA translation in mammalian cells. *Proc. Natl. Acad. Sci.* **101**, 11269–11274 (2004).
44. Novoa, I., Zeng, H., Harding, H. P. & Ron, D. Feedback inhibition of the unfolded protein response by GADD34-mediated dephosphorylation of eIF2alpha. *J. Cell Biol.* **153**, 1011–22 (2001).
45. Wortel, I. M. N., van der Meer, L. T., Kilberg, M. S. & van Leeuwen, F. N. Surviving Stress: Modulation of ATF4-Mediated Stress Responses in Normal and Malignant Cells. *Trends Endocrinol. Metab.* **28**, 794–806 (2017).
46. Hoozemans, J. J. M. *et al.* Activation of the unfolded protein response in Parkinson's disease. *Biochem. Biophys. Res. Commun.* **354**, 707–711 (2007).
47. Hoozemans, J. J. M., Van Haastert, E. S., Nijholt, D. A. T., Rozemuller, A. J. M. & Scheper, W. Activation of the unfolded protein response is an early event in Alzheimer's and Parkinson's disease. *Neurodegener. Dis.* **10**, 212–215 (2012).
48. Bugallo, R. *et al.* Fine tuning of the unfolded protein response by ISRIB improves neuronal survival in a model of amyotrophic lateral sclerosis. *Cell Death Dis.* **11**,

(2020).

49. Shacham, T., Sharma, N. & Lederkremer, G. Z. Protein Misfolding and ER Stress in Huntington's Disease. *Front. Mol. Biosci.* **6**, (2019).
50. Spillantini, M. G., Crowther, R. A., Jakes, R., Hasegawa, M. & Goedert, M. alpha-Synuclein in filamentous inclusions of Lewy bodies from Parkinson's disease and dementia with lewy bodies. *Proc. Natl. Acad. Sci. U. S. A.* **95**, 6469–73 (1998).
51. Adamowicz, D. H. *et al.* Hippocampal α -Synuclein in Dementia with Lewy Bodies Contributes to Memory Impairment and Is Consistent with Spread of Pathology. *J. Neurosci.* **37**, 1675–1684 (2017).
52. Sugeno, N. *et al.* Serine 129 phosphorylation of α -synuclein induces unfolded protein response-mediated cell death. *J. Biol. Chem.* **283**, 23179–23188 (2008).
53. Chung, C. Y. *et al.* Identification and Rescue of a-Synuclein Toxicity in Parkinson Patient-Derived Neurons. *Science (80-.).* **342**, 983–987 (2013).
54. Colla, E. *et al.* Endoplasmic Reticulum Stress Is Important for the Manifestations of a-Synucleinopathy In Vivo. *J. Neurosci.* **32**, 3306–3320 (2012).
55. Colla, E. *et al.* Accumulation of Toxic a-Synuclein Oligomer within Endoplasmic Reticulum Occurs in a-Synucleinopathy In Vivo. *J. Neurosci.* **32**, 3301–3305 (2012).
56. Bellucci, A. *et al.* Induction of the unfolded protein response by a-synuclein in experimental models of Parkinson's disease. *J. Neurochem.* **116**, 588–605 (2011).

57. Heman-Ackah, S. M. *et al.* Alpha-synuclein induces the unfolded protein response in Parkinson's disease SNCA triplication iPSC-derived neurons. *Hum. Mol. Genet.* **26**, 4441–4450 (2017).
58. Aime, P. *et al.* Trib3 Is Elevated in Parkinson's Disease and Mediates Death in Parkinson's Disease Models. *J. Neurosci.* **35**, 10731–10749 (2015).
59. Gully, J. C. *et al.* Up-regulation of activating transcription factor 4 induces severe loss of dopamine nigral neurons in a rat model of Parkinson's disease. *Neurosci. Lett.* **627**, 36–41 (2016).
60. Mercado, G. *et al.* Targeting PERK signaling with the small molecule GSK2606414 prevents neurodegeneration in a model of Parkinson's disease. *Neurobiol. Dis.* **112**, 136–148 (2018).
61. Gorbatyuk, M. S. *et al.* Glucose regulated protein 78 diminishes α -synuclein neurotoxicity in a rat model of parkinson disease. *Mol. Ther.* **20**, 1327–1337 (2012).
62. Sun, X. *et al.* ATF4 Protects Against Neuronal Death in Cellular Parkinson's Disease Models by Maintaining Levels of Parkin. *J. Neurosci.* **33**, 2398–2407 (2013).
63. Ren, B. *et al.* Comparative proteomics reveals the neurotoxicity mechanism of ER stressors tunicamycin and dithiothreitol. *Neurotoxicology* **68**, 25–37 (2018).
64. Helenius, A. & Aebi, M. Roles of N-linked glycans in the endoplasmic reticulum. *Annu. Rev. Biochem.* **73**, 1019–1049 (2004).

65. Wang, H. *et al.* Tunicamycin-induced unfolded protein response in the developing mouse brain. *Toxicol. Appl. Pharmacol.* **283**, 157–167 (2015).
66. Cóppola-Segovia, V. *et al.* ER Stress Induced by Tunicamycin Triggers α -Synuclein Oligomerization, Dopaminergic Neurons Death and Locomotor Impairment: a New Model of Parkinson's Disease. *Mol. Neurobiol.* **54**, 5798–5806 (2017).
67. Jiang, P. *et al.* ER stress response plays an important role in aggregation of α -synuclein. *Mol Neurodegener* **5**, 56 (2010).
68. Leggett, C. *et al.* Tunicamycin produces TDP-43 cytoplasmic inclusions in cultured brain organotypic slices. *J. Neurol. Sci.* **317**, 66–73 (2012).
69. Treiman, M., Caspersen, C. & Christensen, S. B. A tool coming of age: Thapsigargin as an inhibitor of sarco-endoplasmic reticulum Ca^{2+} -ATPases. *Trends Pharmacol. Sci.* **19**, 131–135 (1998).
70. Carreras-Sureda, A., Pihán, P. & Hetz, C. Calcium signaling at the endoplasmic reticulum: fine-tuning stress responses. *Cell Calcium* **70**, 24–31 (2018).
71. Thastrup, O., Cullen, P. J., Drobak, B. K., Hanley, M. R. & Dawson, A. P. Thapsigargin, a tumor promoter, discharges intracellular Ca^{2+} stores by specific inhibition of the endoplasmic reticulum Ca^{2+} -ATPase. *Proc. Natl. Acad. Sci. U. S. A.* **87**, 2466–2470 (1990).
72. Sehgal, P. *et al.* Inhibition of the sarco/endoplasmic reticulum (ER) Ca^{2+} -ATPase by thapsigargin analogs induces cell death via ER Ca^{2+} depletion and the unfolded

- protein response. *J. Biol. Chem.* **292**, 19656–19673 (2017).
73. Stockwell, S. R. *et al.* Mechanism-based screen for G1/S checkpoint activators identifies a selective activator of EIF2AK3/PERK signalling. *PLoS One* **7**, (2012).
 74. Nadanaka, S., Yoshida, H., Kano, F., Murata, M. & Mori, K. Activation of Mammalian Unfolded Protein Response Is Compatible with the Quality Control System Operating in the Endoplasmic Reticulum. *Mol. Biol. Cell* **15**, 2537–2548 (2004).
 75. Kim, S. M. *et al.* Activation of eukaryotic initiation factor-2 α -kinases in okadaic acid-treated neurons. *Neuroscience* **169**, 1831–1839 (2010).
 76. Boyce, M. A Selective Inhibitor of eIF2 Dephosphorylation Protects Cells from ER Stress. *Science (80-.)*. **307**, 935–939 (2005).
 77. Das, I. *et al.* Preventing proteostasis diseases by selective inhibition of a phosphatase regulatory subunit. *Science (80-.)*. **348**, (2015).
 78. Guthrie, L. N. *et al.* Attenuation of PERK signaling selectively controls endoplasmic reticulum stress induced inflammation without compromising immunological responses. *J. Biol. Chem.* **291**, 15830–15840 (2016).
 79. Zhang, L. *et al.* Activation of PERK kinase in neural cells by proteasome inhibitor treatment. *J. Neurochem.* **112**, 238–245 (2010).
 80. Bergmann, T. J. *et al.* Chemical stresses fail to mimic the unfolded protein response resulting from luminal load with unfolded polypeptides. *J. Biol. Chem.* **293**, 5600–

5612 (2018).

81. Sebastian, R. M. & Shoulders, M. D. Chemical Biology Framework to Illuminate Proteostasis. *Annu. Rev. Biochem.* **89**, annurev-biochem-013118-111552 (2020).
82. Lajoie, P., Fazio, E. N. & Snapp, E. L. Approaches to imaging unfolded secretory protein stress in living cells. *Endoplasmic Reticulum Stress Dis.* **1**, 27–39 (2014).
83. Origel Marmolejo, C. A., Bachhav, B., Patibandla, S. D., Yang, A. L. & Segatori, L. A gene signal amplifier platform for monitoring the unfolded protein response. *Nat. Chem. Biol.* **16**, 520–528 (2020).
84. Walter, F., Schmid, J., Dussmann, H., Concannon, C. G. & Prehn, J. H. M. Imaging of single cell responses to ER stress indicates that the relative dynamics of IRE1/XBP1 and PERK/ATF4 signalling rather than a switch between signalling branches determine cell survival. *Cell Death Differ.* **22**, 1502–1516 (2015).
85. Yang, H., Niemeijer, M., van de Water, B. & Beltman, J. B. ATF6 Is a Critical Determinant of CHOP Dynamics during the Unfolded Protein Response. *iScience* **23**, 100860 (2020).
86. Iwawaki, T., Akai, R., Kohno, K. & Miura, M. A transgenic mouse model for monitoring endoplasmic reticulum stress. *Nat. Med.* **10**, 98–102 (2004).
87. Chaveroux, C. *et al.* In vivo imaging of the spatiotemporal activity of the eIF2 - ATF4 signaling pathway: Insights into stress and related disorders. *Sci. Signal.* **8**, rs5–rs5 (2015).

88. Iwawaki, T. *et al.* Transgenic mouse model for imaging of ATF4 translational activation-related cellular stress responses in vivo. *Sci. Rep.* **7**, 1–9 (2017).
89. Gordon, J., Amini, S. & White, M. K. *Neuronal Cell Culture*. **1078**, (Humana Press, 2013).
90. Santiago-Lopez, A. J., Gutekunst, C.-A. & Gross, R. E. C3 transferase gene therapy for continuous RhoA inhibition. in *Rho GTPases* (ed. Rivero, F.) 267–281 (Humana Press, 2018). doi:10.1007/978-1-4939-8612-5
91. Grieger, J. C., Choi, V. W. & Samulski, R. J. Production and characterization of adeno-associated viral vectors. *Nat. Protoc.* **1**, 1412–1428 (2006).
92. Gupta, R. V., Santiago-Lopez, A. J., Berglund, K., Gross, R. E. & Gutekunst, C.-A. N. In Vivo Assessment of Cell Death and Nigrostriatal Pathway Integrity Following Continuous Expression of C3 Transferase. *Neuroscience* **442**, 183–192 (2020).
93. Karra, D. & Dahm, R. Transfection techniques for neuronal cells. *J. Neurosci.* **30**, 6171–6177 (2010).
94. Deverman, B. E., Ravina, B. M., Bankiewicz, K. S., Paul, S. M. & Sah, D. W. Y. Gene therapy for neurological disorders: progress and prospects. *Nat. Rev. Drug Discov.* (2018). doi:10.1038/nrd.2018.110
95. Grimm, D. *et al.* In Vitro and In Vivo Gene Therapy Vector Evolution via Multispecies Interbreeding and Retargeting of Adeno-Associated Viruses. *J. Virol.* **82**, 5887–5911 (2008).

96. Guan, B. J. *et al.* A Unique ISR Program Determines Cellular Responses to Chronic Stress. *Mol. Cell* **68**, 885-900.e6 (2017).
97. Bedford, L., Paine, S., Sheppard, P. W., Mayer, R. J. & Roelofs, J. Assembly, structure, and function of the 26S proteasome. *Trends Cell Biol.* **20**, 391–401 (2010).
98. Chang, K. H. *et al.* Impairment of proteasome and anti-oxidative pathways in the induced pluripotent stem cell model for sporadic Parkinson's disease. *Park. Relat. Disord.* **24**, 81–88 (2016).
99. Fricker, L. D. Proteasome Inhibitor Drugs. *Annu. Rev. Pharmacol. Toxicol.* **60**, 457–476 (2020).
100. Goldberg, A. L. Development of proteasome inhibitors as research tools and cancer drugs. *J. Cell Biol.* **199**, 583–588 (2012).
101. Wang, J. *et al.* Hyperphosphorylation and accumulation of neurofilament proteins in Alzheimer disease brain and in okadaic acid-treated SY5Y cells. *FEBS Lett.* **507**, 81–87 (2001).
102. Goldbaum, O. & Richter-Landsberg, C. Activation of PP2A-like phosphatase and modulation of tau phosphorylation accompany stress-induced apoptosis in cultured oligodendrocytes. *Glia* **40**, 271–282 (2002).
103. Mills, J. C., Lee, V. M. Y. & Pittman, R. N. Activation of a PP2A-like phosphatase and dephosphorylation of τ protein characterize onset of the execution phase of apoptosis. *J. Cell Sci.* **111**, 625–636 (1998).

104. Ho, Y.-S. *et al.* Endoplasmic reticulum stress induces tau pathology and forms a vicious cycle: implication in Alzheimer's disease pathogenesis. *J. Alzheimer's Dis. JAD* **28**, 839–54 (2012).
105. Kamat, P. K., Rai, S., Swarnkar, S., Shukla, R. & Nath, C. Molecular and cellular mechanism of okadaic acid (OKA)-induced neurotoxicity: a novel tool for Alzheimer's disease therapeutic application. *Mol. Neurobiol.* **50**, 852–865 (2014).
106. Lashuel, H. A., Overk, C. R., Oueslati, A. & Masliah, E. The many faces of α -synuclein: from structure and toxicity to therapeutic target. *Nat. Rev. Neurosci.* **14**, 38–48 (2012).
107. Goedert, M., Jakes, R. & Spillantini, M. G. The Synucleinopathies: Twenty Years on. *J. Parkinsons. Dis.* **7**, S53–S71 (2017).
108. Conway, K. A., Harper, J. D. & Lansbury, P. T. Fibrils formed in vitro from α -synuclein and two mutant forms linked to Parkinson's disease are typical amyloid. *Biochemistry* **39**, 2552–2563 (2000).
109. Giasson, B. I., Murray, I. V. J., Trojanowski, J. Q. & Lee, V. M. Y. A Hydrophobic Stretch of 12 Amino Acid Residues in the Middle of α -Synuclein Is Essential for Filament Assembly. *J. Biol. Chem.* **276**, 2380–2386 (2001).
110. Goedert, M., Spillantini, M. G., Del Tredici, K. & Braak, H. 100 years of Lewy pathology. *Nat. Rev. Neurol.* **9**, 13–24 (2013).
111. Siddiqui, I. J., Pervaiz, N. & Abbasi, A. A. The Parkinson Disease gene SNCA:

- Evolutionary and structural insights with pathological implication. *Sci. Rep.* **6**, 24475 (2016).
112. Colla, E. *et al.* Accumulation of Toxic α -Synuclein Oligomer within Endoplasmic Reticulum Occurs in α -Synucleinopathy In Vivo. *J. Neurosci.* **32**, 3301–3305 (2012).
 113. Santiago-Lopez, A. J., Gutekunst, C.-A. & Gross, R. E. C3 transferase gene therapy for continuous RhoA inhibition. in *Rho GTPases* (ed. Rivero, F.) (Humana Press, 2018). doi:10.1007/978-1-4939-8612-5
 114. Deger, J. M., Gerson, J. E. & Kaye, R. The interrelationship of proteasome impairment and oligomeric intermediates in neurodegeneration. *Aging Cell* **14**, 715–724 (2015).
 115. David, D. C. *et al.* Proteasomal degradation of tau protein. *J. Neurochem.* **83**, 176–185 (2002).
 116. Niepel, M., Spencer, S. L. & Sorger, P. K. Non-genetic cell-to-cell variability and the consequences for pharmacology. *Curr. Opin. Chem. Biol.* **13**, 556–561 (2009).
 117. Polymeropoulos, M. *et al.* Mutation in the α -Synuclein Gene Identified in Families with Parkinson's Disease. *Science* (80-.). **276**, 2045–2047 (1997).
 118. Conway, K. A., Harper, J. D. & Lansbury, P. T. Accelerated in vitro fibril formation by a mutant α -synuclein linked to early-onset Parkinson disease. *Nat. Med.* **4**, 1318–1320 (1998).

119. Ip, C. W. *et al.* AAV1/2-induced overexpression of A53T- α -synuclein in the substantia nigra results in degeneration of the nigrostriatal system with Lewy-like pathology and motor impairment: a new mouse model for Parkinson's disease. *Acta Neuropathol. Commun.* **5**, 11 (2017).
120. Li, L. *et al.* Human A53T α -synuclein causes reversible deficits in mitochondrial function and dynamics in primary mouse cortical neurons. *PLoS One* **8**, (2013).
121. Hamdan, N., Kritsiligkou, P. & Grant, C. M. ER stress causes widespread protein aggregation and prion formation. *J. Cell Biol.* **216**, 2295–2304 (2017).
122. Panchision, D. M. *et al.* An Immortalized, Type-1 Astrocyte of Mesencephalic Origin Source of a Dopaminergic Neurotrophic Factor. *J. Mol. Neurosci.* **11**, 209–222 (1998).
123. Petrova, P. S. *et al.* MANF: A new mesencephalic, astrocyte-derived neurotrophic factor with selectivity for dopaminergic neurons. *J. Mol. Neurosci.* **20**, 173–187 (2003).
124. Henderson, M. J., Richie, C. T., Airavaara, M., Wang, Y. & Harvey, B. K. Mesencephalic astrocyte-derived neurotrophic factor (MANF) secretion and cell surface binding are modulated by KDEL receptors. *J. Biol. Chem.* **288**, 4209–4225 (2013).
125. Yan, Y., Rato, C., Rohland, L., Preissler, S. & Ron, D. MANF antagonizes nucleotide exchange by the endoplasmic reticulum chaperone BiP. *Nat. Commun.* **10**, (2019).

126. Pakarinen, E. *et al.* MANF ablation causes prolonged activation of the UPR without neurodegeneration in the mouse midbrain dopamine system. *eNeuro* **7**, (2020).
127. Hao, F. *et al.* Long-term protective effects of AAV9-mesencephalic astrocyte-derived neurotrophic factor gene transfer in parkinsonian rats. *Exp. Neurol.* **291**, 120–133 (2017).
128. Xu, S. *et al.* Mesencephalic astrocyte-derived neurotrophic factor (MANF) protects against A β toxicity via attenuating A β -induced endoplasmic reticulum stress. *J. Neuroinflammation* **16**, 1–14 (2019).
129. Hellman, M. *et al.* Mesencephalic astrocyte-derived neurotrophic factor (MANF) has a unique mechanism to rescue apoptotic neurons. *J. Biol. Chem.* **286**, 2675–2680 (2011).
130. Tseng, K. Y. *et al.* MANF Promotes Differentiation and Migration of Neural Progenitor Cells with Potential Neural Regenerative Effects in Stroke. *Mol. Ther.* **26**, 238–255 (2018).
131. Mätlik, K. *et al.* Poststroke delivery of MANF promotes functional recovery in rats. *Sci. Adv.* **4**, 1–8 (2018).
132. Voutilainen, M. H. *et al.* Mesencephalic astrocyte-derived neurotrophic factor is neurorestorative in rat model of Parkinson's disease. *J. Neurosci.* **29**, 9651–9659 (2009).
133. Cordero-Llana, Ó. *et al.* Enhanced efficacy of the CDNF/MANF family by

- combined intranigral overexpression in the 6-OHDA rat model of parkinson's disease. *Mol. Ther.* **23**, 244–254 (2015).
134. Richman, C. *et al.* C. elegans MANF Homolog Is Necessary for the Protection of Dopaminergic Neurons and ER Unfolded Protein Response. *Front. Neurosci.* **12**, 1–11 (2018).
 135. Wang, S. & Kaufman, R. J. The impact of the unfolded protein response on human disease. *J. Cell Biol.* **197**, 857–867 (2012).
 136. Mazroui, R., Di Marco, S., Kaufman, R. J. & Gallouzi, I.-E. Inhibition of the Ubiquitin-Proteasome System Induces Stress Granule Formation. *Mol. Biol. Cell* **18**, 2603–2618 (2007).
 137. Spillantini, M. G., Crowther, R. A., Jakes, R., Hasegawa, M. & Goedert, M. alpha-Synuclein in filamentous inclusions of Lewy bodies from Parkinson's disease and dementia with lewy bodies. *Proc. Natl. Acad. Sci. U. S. A.* **95**, 6469–73 (1998).
 138. Prots, I. *et al.* α -Synuclein oligomers induce early axonal dysfunction in human iPSC-based models of synucleinopathies. *Proc. Natl. Acad. Sci.* 201713129 (2018). doi:10.1073/pnas.1713129115
 139. Winner, B. *et al.* In vivo demonstration that a-synuclein oligomers are toxic. *Proc. Natl. Acad. Sci.* **108**, 4194–4199 (2011).
 140. Ordonez, D. G., Lee, M. K. & Feany, M. B. α -synuclein Induces Mitochondrial Dysfunction through Spectrin and the Actin Cytoskeleton. *Neuron* **97**, 108-124.e6

(2018).

141. Klaips, C. L., Jayaraj, G. G. & Hartl, F. U. Pathways of cellular proteostasis in aging and disease. *J. Cell Biol.* **217**, 51–63 (2018).
142. Pintado, C., MacÍas, S., Domínguez-Martín, H., Castanõ, A. & Ruano, Di. Neuroinflammation alters cellular proteostasis by producing endoplasmic reticulum stress, autophagy activation and disrupting ERAD activation. *Sci. Rep.* **7**, 1–12 (2017).
143. Shpilka, T. & Haynes, C. M. The mitochondrial UPR: mechanisms, physiological functions and implications in ageing. *Nat. Rev. Mol. Cell Biol.* **19**, 109–120 (2018).
144. Baleriola, J. *et al.* Axonally synthesized ATF4 transmits a neurodegenerative signal across brain regions. *Cell* **158**, 1159–1172 (2014).
145. Varley, A. W. & Munford, R. S. Physiologically responsive gene therapy. *Mol. Med. Today* **4**, 445–451 (1998).
146. Vasquez, V., Mitra, J., Perry, G., Rao, K. S. & Hegde, M. L. An Inducible Alpha-Synuclein Expressing Neuronal Cell Line Model for Parkinson’s Disease1. *J. Alzheimer’s Dis.* **66**, 453–460 (2018).
147. Volpicelli-Daley, L. A., Luk, K. C. & Lee, V. M.-Y. Addition of exogenous α -synuclein preformed fibrils to primary neuronal cultures to seed recruitment of endogenous α -synuclein to Lewy body and Lewy neurite-like aggregates. *Nat. Protoc.* **9**, 2135–2146 (2014).

148. Gutekunst, C.-A., Tung, J. K., McDougal, M. E. & Gross, R. E. C3 transferase gene therapy for continuous conditional RhoA inhibition. *Neuroscience* **339**, 308–318 (2016).
149. Carpenter, A. E. *et al.* CellProfiler: Image analysis software for identifying and quantifying cell phenotypes. *Genome Biol.* **7**, (2006).